D_2 Receptors Receive Paracrine Neurotransmission and Are Consistently Targeted to a Subset of Synaptic Structures in an Identified Neuron of the Crustacean Stomatogastric Nervous System

Max F. Oginsky, Edmund W. Rodgers, Merry C. Clark, Robert Simmons, Wulf-Dieter C. Krenz, and Deborah J. Baro*
Department of Biology, Georgia State University, Atlanta, Georgia 30303

ABSTRACT

Dopamine (DA) modulates motor systems in phyla as diverse as nematodes and arthropods up through chordates. A comparison of dopaminergic systems across a broad phylogenetic range should reveal shared organizing principles. The pyloric network, located in the stomatogastric ganglion (STG), is an important model for neuromodulation of motor networks. The effects of DA on this network have been well characterized at the circuit and cellular levels in the spiny lobster, *Panulirus interruptus*. Here we provide the first data about the physical organization of the DA signaling system in the STG and the function of D_2 receptors in pyloric neurons. Previous studies showed that DA altered intrinsic firing properties and synaptic output in the pyloric dilator (PD) neuron, in part by reducing calcium currents and increasing outward potassium currents. We performed single cell reverse transcriptase-polymerase chain reaction (RT-PCR) experiments to show that PD neurons exclusively expressed a type 2 ($D_{2\alpha Pan}$) DA receptor. This was confirmed by using confocal microscopy in conjunction with immunohistochemistry (IHC) on STG whole-mount preparations containing dye-filled PD neurons. Immunogold electron microscopy showed that surface receptors were concentrated in fine neurites/terminal swellings and vesicle-laden varicosities in the synaptic neuropil. Double-label IHC experiments with tyrosine hydroxylase antiserum suggested that the $D_{2\alpha Pan}$ receptors received volume neurotransmissions. Receptors were further mapped onto three-dimensional models of PD neurons built from Neurolucida tracings of confocal stacks from the IHC experiments. The data showed that $D_{2\alpha Pan}$ receptors were selectively targeted to approximately 40% of synaptic structures in any given PD neuron, and were nonuniformly distributed among neurites. J. Comp. Neurol. 518:255–276, 2010.

INDEXING TERMS: dopamine; medium spiny neuron; receptor distribution; immunohistochemistry; single cell PCR; tyrosine hydroxylase; invertebrate

Dopamine (DA) modulates motor function throughout the animal kingdom by acting on a limited number of highly conserved receptors in a large assortment of cell types. The extent to which receptor function varies among subcellular compartments, cell types, and species is an important consideration that speaks to the organizing principles and evolution of modulatory systems. A receptor's function is largely determined by its associated signal transduction cascades and ultimate targets (i.e., the receptor signaling network), by the modes of transmission it receives, and by its subcellular distribution.

A given DA receptor (DAR) can indirectly modulate a variety of target proteins by directly activating multiple cascades that begin with Gα and Gβγ subunits (Neve et al., 2004) and β-arrestin desensitization (Masri et al., 2008; Beaulieu et al., 2009). DARs can also modulate tar-

Additional Supporting Information may be found in the online version of this article.

Grant sponsor: National Institutes of Health; Grant number: DA-024039 (to D.J.B.); Grant sponsor: Molecular Basis of Disease; Grant number: fellowship (to M.C.C.).

The first three authors contributed equally to this paper.

Dr. Clark's current address: Georgia Highlands College, Floyd Campus, 3175 Cedartown Highway, SE, Rome, GA 30161.
E-mail: mclark@highlands.edu

*CORRESPONDENCE TO: Deborah J. Baro, Department of Biology, Georgia State University, 24 Peachtree Center Ave., Atlanta, GA 30303.
E-mail: dbaro@gsu.edu

Received 15 May 2009; Revised 4 July 2009; Accepted 8 September 2009
DOI 10.1002/cne.22225
Published online September 16, 2009 in Wiley InterScience (www.interscience.wiley.com).

get proteins by direct physical interactions (Cepeda and Levine, 2006). The fact that scaffold and adaptor proteins assemble individual signaling molecules into larger signaling complexes (Collins and Grant, 2007), and that scaffold/adaptor protein binding domains and their respective motifs can be evolutionarily preserved (Ullah et al., 2008), begs the question: Are DAR signaling networks well conserved? Defining receptor function in a variety of cell types will complement the current bioinformatic efforts to identify evolutionarily conserved protein interaction networks (Guo and Hartemink, 2009; Zaslavskiy et al., 2009).

A variety of DA transmissions differentially effect receptor activation. DA can act as a neurohormone or a neurotransmitter. DA neurotransmission can be classified as either wired or volume (Zoli et al., 1998; Agnati et al., 2006; Goto et al., 2007; Schultz, 2007). Wired transmission is characterized by point-to-point contacts between a presynaptic active zone and a postsynaptic density separated by a narrow synaptic cleft. Volume transmission is characterized by open synapses that favor the diffusion of DA for large distances beyond the synaptic cleft and into the surrounding extracellular fluid. Volume transmission is energy efficient, but fairly nonspecific. Specificity is determined by the placement of DA reuptake mechanisms and receptors.

Neuronal DARs can be specifically targeted to subcellular compartments where they can serve different functions (Yao et al., 2008). For example, in striatal medium spiny neurons (MSNs) DARs are precisely localized on postsynaptic structures. Whereas presynaptic glutamatergic terminals contact the apexes of MSN postsynaptic spines, DARs reside on the necks of the spines (Hersch et al., 1995; Yung et al., 1995). Moreover, there are data to suggest that receptors may be targeted to a subset of synapses on a given neuron. Both cortical and hippocampal presynaptic glutamatergic inputs converge onto the postsynaptic spines of a single MSN in the ventral striatum, but pharmacological and electrophysiological data suggest that postsynaptic D_1 receptors modulate hippocampal, but not cortical input (Goto and Grace, 2005, 2008).

DAR function has been delineated in components of mammalian motor systems, such as the striatum (Schultz, 2007; Surmeier et al., 2007; Kreitzer and Malenka, 2008). However, little is known about DAR function in otherwise well-characterized invertebrate motor systems. The crustacean stomatogastric nervous system (STNS) is a small motor system that has long served as a useful model for the study of motor pattern generation and modulation (Fig. 1). Neurons in the STNS are assembled into multiple well-defined central pattern generators (CPGs) that drive different sets of muscles to produce a patterned activity associated with a specific function (Marder and Bucher, 2006). The effects of DA are especially well characterized for the pyloric network (Harris-Warrick et al., 1998), a CPG that resides exclusively within the stomatogastric ganglion (STG; Fig. 1). DA acts as a neurohormone and a neuromodulator in the STNS. A literature-based composite of DA-containing cells in the STNS, and dopaminergic inputs to the STG, is shown in Figure 1. It appears that dopaminergic inputs to the pyloric network exclusively stem from a few cells in the commissural ganglia (Goldstone and Cooke, 1971; Sullivan et al., 1977; Kushner and Barker, 1983; Pulver and Marder, 2002; Pulver et al., 2003; Tierney et al., 2003 and references therein).

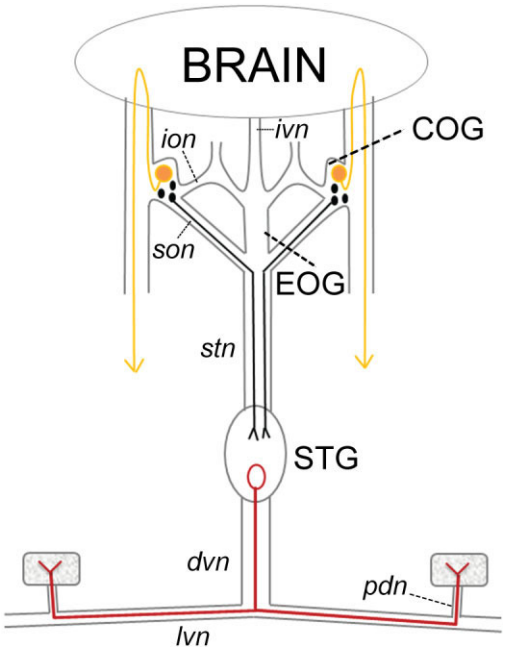

Figure 1. The stomatogastric nervous system (STNS). Diagram of the STNS and connection to the brain. Nerves are drawn as lines and rectangles, muscles as stippled squares, dopamine-containing neurons as filled circles, and the pyloric dilator (PD) neuron as an open circle. The STNS comprises four ganglia: the two commissural ganglia (COGs), the esophageal ganglion (EOG), and the stomatogastric ganglion (STG). The PD neuron, located in the STG, projects an axon down the dorsal ventricular nerve (*dvn*). The axon bifurcates prior to entering the lateral ventricular nerves (*lvn*) and continues to run through the pyloric dilator nerves (pdn) to innervate the two PD muscles. Small DA-containing neurons in the COGs can project axons through the superior esophageal nerve (*son*) and down the stomatogastric nerve (*stn*) to terminate in the STG. The large L-cells in the COGs project to the ventral surface of the brain, whereupon axons reverse direction and ultimately terminate in ipsilateral pericardial organs, which release neuromodulators into the hemolymph (indicated by arrowheads). Not shown are the many dopaminergic cells in the brain (Tierney et al., 2003). In some species, neurons in the STG may also contain DA (Pulver et al., 2003). Dopamine has not been observed in the EOG, the inferior esophageal nerve (*ion*), or the inferior ventricular nerve (*ivn*) that connects the brain to the STNS.

Knowledge of DAR function in the STNS would not only enhance our understanding of dopaminergic modulation of a motor circuit, but would also permit comparisons of receptor function in defined cell types across species. We recently cloned and characterized the three known arthropod DARs from the spiny lobster, *Panulirus interruptus* (Clark and Baro, 2006, 2007). All three receptors were expressed in the STG and activated distinct transduction cascades in STNS membrane preparations (Clark et al., 2008). Here we describe DAR expression, subcellular localization, and DA neurotransmission for a single identified cell type in the spiny lobster pyloric network.

MATERIALS AND METHODS

Animals

Pacific spiny lobsters (*P. interruptus*) were obtained from Don Tomlinson Commercial Fishing (San Diego, CA). Lobsters were maintained at 16°C in constantly aerated and filtered seawater. Animals were anesthetized on ice for at least 30 minutes before dissection.

Cell identification

The STNS was dissected and pinned in a Sylgard-lined Petri dish by using standard techniques (Selverston et al., 1976). The stomatogastric ganglion (STG) was desheathed. The preparation was superfused with *Panulirus* saline consisting of (in mM) 479 NaCl, 12.8 KCl, 13.7 $CaCl_2$, 39 Na_2SO_4, 10 $MgSO_4$, 2 glucose, 4.99 HEPES, 5 TES at pH 7.4. Extracellular recordings from the pyloric dilator nerve (pdn), medial ventricular nerve (mvn), and lateral ventricular nerve (lvn) were obtained with stainless steel pin electrodes and a differential AC amplifier (A-M Systems, Everett, WA) as previously described (Baro et al., 1997). Intracellular somatic recordings were obtained by using glass microelectrodes filled with 3 M KCl (20–30 MΩ) and an Axoclamp 2B amplifier (Axon Instruments, Foster City, CA). Neurons were identified by correlating action potentials from somatic intracellular recordings with extracellularly recorded action potentials on identified motor nerves, and by their characteristic shape and timing of oscillations.

Single cell RT-PCR

Electrophysiologically identified PD cells were removed from the STG following Baro et al. (1996), with modifications. The ganglion was incubated with 1.2 mg/ml of collagenase type IA (Sigma-Aldrich, St. Louis, MO) until the cells were amenable to extraction with a fire-polished microelectrode. Cells were immediately placed on dry ice and stored at −80°C until reverse transcription. PD cells with the glial cap intact (n = 8) and glial cap removed (n = 5) were processed for RT-PCR by using a modified cells-to-cDNA kit protocol (Ambion, Austin, TX). First, 9 μl of lysis buffer was added to the cell and incubated at 75°C for 10 minutes. Next, 0.2 μl of DNase 1 was added to lysis buffer and incubated for 15 minutes at 37°C, and then again at 75°C for an additional 5 minutes for inactivation. RNA was then reverse transcribed as per the manufacturer's instructions. The resulting first-strand cDNA for a given cell was then aliquotted into four tubes, each containing a primer set for either $D_{1\alpha Pan}$, $D_{1\beta Pan}$, $D_{2\alpha Pan}$, or α-tubulin. Then 2 μl from the reverse transcription reaction were added to 23 μl of PCR mix containing Advantage Taq polymerase (ClonTech, Palo Alto, CA), and used according to the manufacturer's instructions. All reactions for each cell were run simultaneously under the following PCR conditions: 95°C for 1 minute, 60°C for 1 minute, 68°C for 45 seconds, for 45 cycles. PCR products were run on a polyacrylamide gel and visualized with ethidium bromide.

The primers used were as follows:

D1α F 5′-TGTAAATTTGCCAAAGAGAAGAAAGCAGCCAAGACT-3′

D1α R 5′-GACACCGTCGGGGACAGCAGGAGCAGAGGATT-3′

D1β F 5′-TGTGGTGTCCTCGTGCATCAGTTTCTTCC-3′

D1β R 5′-GCACGGGGCGGCCACCTTCTTG-3′

D2 F 5′ GGCATCCCGCTCTTCTTCGTG-3′

D2 R 5′ TTTCTATGACGCTGCCTGCTTTGATTTC-3′

αT F 5′ GACTACGGCAAGAAGAGCAAACT-3′

αT R 5′ TGTTCATGTTCTGCGGCAGATGTC-3′.

Dye fills

Identified PD neurons were filled with a lysine-fixable, dextran-coupled Texas Red fluorophore that cannot pass through gap junctions (M.W. 10,000; Molecular Probes, Eugene, OR) by pressure-injecting a 1% solution of the fluorophore in 0.2 M KCl using 20-msec pulses at 0.05 Hz and 28 psi for 10 minutes. Spontaneous burst activity was monitored throughout this period, and the neuron was used only if there was no significant change in output. The fluorophore diffused for 2–24 hours at room temperature prior to fixation. In several of the initial experiments, just prior to fixation, a microelectrode was used to measure membrane potential, and a fluorescent microscope was used to determine the quality of the fill and the integrity of a neuron. In most cases, neurons showed normal membrane potentials, the dye spread to the terminals throughout the neuropil, and the neuron appeared translucent. In very few instances, we observed dead or dying neurons that appeared opaque, with the spread of dye restricted. In later experiments, neurons were visually inspected prior to fixation, and dead or dying neurons were excluded from analysis.

TABLE 1.
Primary Antibodies

Antigen	Immunogen	Manufacturer, purification, species, type, cat. no.	Concentration/ dilution used
$D_{2\alpha Pan}$ receptor	Two synthetic peptides, aa 33-47 and aa 546-561 from *P. interruptus* as described in Clark et al. (2008)	21st Century Biochemicals, affinity-purified rabbit polyclonal, custom	2 μg/ml
$D_{1\alpha Pan}$ receptor	Synthetic peptide, aa 329-344 from *P. interruptus* as described in Clark et al. (2008)	Bethyl Laboratories, affinity-purified rabbit polyclonal, custom	1 μg/ml
$D_{1\beta Pan}$ receptor	Synthetic peptide, aa 80-99 from *P. interruptus* as described in Clark et al. (2008)	Alpha Diagnostic, affinity-purified rabbit polyclonal, custom	1 μg/ml
Synapsin	*Drosophila* SYNORF1 aa 89-449GST fusion protein, representing the conserved 5′ end of synapsin cDNA, as defined in Klagges et al. (1996).	Developmental Studies Hybridoma Bank (University of Iowa), mouse monoclonal, cat. no. 3C11 concentrate	1:200
Synaptotagmin	Recombinant protein for aa 134-474 from *Drosophila melanogaster* as described in Littleton et al. (1993)	Gift from Dr. Hugo Bellen, rabbit polyclonal serum named DSTY2.	1:1,000
Tyrosine hydroxylase	Tyrosine hydroxylase purified from rat PC12 cells; recognized epitope is from conserved midportion of molecule	ImmunoStar, mouse monoclonal, cat. no. 22941	1:200

Antibody characterization

Antibodies are listed in Table 1. We previously performed several experiments to show that the custom-made, affinity-purified antisera for $D_{2\alpha Pan}$, $D_{1\alpha Pan}$, and $D_{1\beta Pan}$ were specific for their respective receptors (Clark et al., 2008). Each recognized the expected bands on Western blots containing protein extracts from *P. interruptus* nervous tissue, and bands were lost upon preabsorption with the appropriate peptide. Similarly, peptide preabsorption produced diminished signals in IHC experiments. Finally, antibodies specifically blocked the function of their cognate receptor in STNS membrane preparations. The antiserum for synaptotagmin specifically and appropriately labeled 1) bands of the expected molecular weight in Western blot experiments by using protein preparations from crustacean neuromuscular junctions (Cooper et al., 1995); and 2) the axon terminals of spiny lobster neuromuscular junctions in IHC experiments (Clark et al., 2004). The synapsin antibody recognized the appropriate bands on Western blots containing crustacean protein extracts (Sullivan et al., 2007). EM studies also showed that this antibody labeled crustacean synaptic vesicles (Skiebe and Ganeshina, 2000). Additionally, this antibody has been used to label lobster STG synaptic neuropil in IHC experiments (Bucher et al., 2007). It should be noted that, as expected, both presynaptic markers (i.e., anti-synaptotagmin and anti-synapsin) gave similar results and very clearly labeled the anatomically distinct STG synaptic neuropil. The particular antiserum for tyrosine hydroxylase used in this study previously identified the exact same dopaminergic neurons as a TH-*gal4*-driver line in the related arthropod, *Drosophila melanogaster* (Vomel and Wegener, 2008). Antiserum for tyrosine hydroxylase consistently labeled crustacean DA-containing neurons (Cournil et al., 1994, 1995), and this particular antiserum has been used to identify crustacean dopaminergic neurons and inputs to the STG (Pulver and Marder, 2002; Pulver et al., 2003; Fort et al., 2004). Finally, the tyrosine hydroxylase antiserum used here recognized a single band of the appropriate size on Western blots containing protein extracts from *P. interruptus* nervous tissue (n = 3, Suppl. Fig. S1A). Together, these data suggested that the tyrosine hydroxylase antiserum can be used to detect dopaminergic neurons in the spiny lobster STNS.

IHC

Primary antibodies were used in our previously described single- and double-label IHC protocols (Baro et al., 2000; Clark et al., 2004) at the concentrations/dilutions indicated in Table 1. Secondary antibodies (anti-mouse, cat. no. 115-075-003, anti-rabbit, cat. no. 111-075-144; anti-rabbit, cat. no. 111-095-144) were all purchased from Jackson ImmunoResearch (West Grove, PA) and used at a 1:200 dilution. For all IHC experiments, controls were performed such that the primary antibody was omitted or preabsorbed with its peptide antigen. In all cases, no staining was observed in the controls. IHC experiments were usually performed on wholemount preparations. However, in four experiments, fixed ganglia were imbedded in 40°C, 4% low melting point agarose (Sigma, St. Louis, MO) and sectioned (50–70 μm) with a Lancer Series 1000 Vibratome (Vibratome, St. Louis, MO). All sections of a given STG were transferred to PBST-filled wells, and the aforementioned single-label IHC protocol was performed on the floating sections.

Confocal imaging

All confocal images were obtained with a Zeiss LSM510 confocal imaging system (Zeiss, Oberkochen, Germany). Confocal projections were constructed by using the LSM510 Image Examiner or Image Browser software (version 4.2.0.121, Zeiss). Color enhancements were performed with Adobe Photoshop 7.0 software (Adobe Systems, Mountain View, CA). Nonspecific background specks were removed for the extreme high-intensity confocal projection shown in Figure 6B with the Photoshop eraser tool. Channel offset was measured with a Zeiss reference slide containing fluorescent spheres having broad emission/excitation spectra (i.e., each sphere produced a signal in red, green, and blue channels). Spheres were imaged with a 40× oil objective and 3× optical zoom (i.e., same settings as for Fig. 6D). Images for each channel overlaid and there was no significant offset (Suppl. Fig. S1B).

Immunogold electron microscopy (EM)

Immunogold EM studies were performed with an EMS custom ultra small kit containing gold particle-labeled secondary antibodies (Electron Microscopy Sciences [EMS], Ft. Washington, PA) and the $D_{2\alpha Pan}$ primary antibody. Chemicals were obtained from Sigma-Aldrich, and steps were performed at room temperature, unless indicated otherwise. STG wholemount preparations were fixed in 3% paraformaldehyde (EMS), 0.5% glutaraldehyde (EMS), 0.01% DMSO (Tousimis, Rockville, MD) in PBS for 1 hour. Preparations were washed twice in PBS (pH 7.4), and oxidized twice for 10 minutes each by using a DAB-H_2O_2 solution with shaking. Oxidation was stopped by washing in PBS. Aldehydes were inactivated by incubating in 0.05 M glycine in PBS for 15 minutes. Ganglia were then permeablized for 30 minutes by using 0.05% Triton-X in PBS. Preparations were washed 4 times, 10 minutes each, and blocked for 1.5 hours by incubating with AURION goat blocking solution (EMS). Preparations were washed with incubation buffer (bovine serum albumin [BSA]-c/PBS/NaN_3), 3 times, for 5 minutes each. Primary antibody was added to a final concentration of 2 μg/ml in BSA-c buffer, and preparations were incubated overnight at 4°C. Preparations were then washed with BSA-c buffer 4 times, 5 minutes each.

The secondary antibody was added at a 1:100 dilution in BSA-c buffer for 1 hour. Preparations were washed 4 times with BSA-c buffer and twice with PBS, for 5 minutes each. Ganglia were postfixed in 2% glutaraldehyde in PBS for 5 minutes and washed with distilled water 3 times, for 5 minutes each with shaking. Silver enhancement was performed for 15 minutes by using R Gent SE-EM (EMS) in the dark. Preparations were washed 5 times over 5 minutes in distilled water, followed by a second postfixation with 1% OsO_4. Preparations were washed 3 times with distilled water, and then dehydrated in a graded ethanol series (30, 50, 70, 90, 100, and 100% for 10 minutes each). The preparation was infiltrated with LR White Resin (London Resin Co, Reading, UK) overnight and polymerized in gelatin capsules at 60°C for 24 hours. Sections were cut with an RMC MT-X ultramicrotome diamond knife, collected on 300-mesh nickel grids, and imaged with a LEO 906e transmission electron microscope operating at kV80. Control experiments (i.e., preabsorption of primary antibody with peptide antigen) were also performed. Gold particles were completely absent in control blocs.

We determined the average packing density of gold particles per μm^2 of plasmalemma for three different profile areas. Axiovision software (Olympus) was used to measure the length of membrane around 30 neurites > 1.5 μm, 30 neurites < 1.5 μm, and 22 vesicle-containing varicosities. The number of gold particles within 20 nm of either side of the plasmalemma was counted for each structure. Density was determined by dividing the number of particles by area (membrane length × 40 nm). Significant differences were determined with a Kruskal-Wallis test followed by a Dunn's multiple comparison post hoc test.

Three-dimensional (3D) reconstruction and analysis of PD neurons

A $D_{2\alpha Pan}$ IHC experiment was performed on a wholemount containing a single dye-filled PD neuron as described above. To render a 3D model of the PD neuron, and map receptor distribution within it, we obtained overlapping confocal stacks (13–17 stacks per animal) that included the entire neuron, up to the point where the axon exited the STG via the dvn ($n = 3$ neurons). Each stack was comprised of a continuous series of 1-μm dorsal to ventral confocal slices. The z-series steps were such that there were no gaps between slices. After imaging the entire neuron, the stacks were imported into the Neurolucida imaging software package (MicroBrightField, Williston, VT). Neurolucida was used to trace the PD neuron manually, keeping the length and diameter of the soma and all traced neurites matched to the actual filled structures. Neurolucida compiled volume measurements for each traced structure, and recorded the 3D position of each branch origin and ending. These values were then imported into the NeuroExplorer software program (MicroBrightField), which constructed a morphological model of the cell as a composition of cylinders. A comparison of volumes calculated from confocal images (Zeiss LSM510 software) versus Neurolucida tracings suggests that we traced 87–94% of a given neuron (Table 2).

We designated a hierarchal branch order based on point of origin: secondary branches arose from a single primary neurite, which emerged from the soma and left the STG

TABLE 2.
Pyloric Dilator (PD) Neuron Volumes

	Volume of 3D tracing (μm^3)	Confocal volume (μm^3)	% Traced	Length of primary neurite (μm)
PD-1	3.7×10^5	4.1×10^5	89	766.2
PD-2	4.7×10^5	5.5×10^5	87	1,167.4
PD-3	4.1×10^5	4.4×10^5	94	1,015.1

posteriorly. Secondary branches gave rise solely to tertiary branches, which then gave rise to quaternary, and so on. Similar to Bucher et al. (2007), we observed cases in which two or more secondary branches emerged from the primary neurite at an enlarged region containing multiple nodes. These were less extensive than the "hand-like" branching structure, described for *Homarus americanus*, however, and we were able to clearly identify the branch origin point for all secondary branches.

When tracing the finest neurites (<1 μm diameter), it was occasionally not obvious where the branch originated and/or ended. Branches were only traced if the origin and ending were clear. Questionable neurites were either left untraced, or were traced as far as they could be seen.

As a PD neuron was traced, markers were placed to indicate the presence or the absence of varicosities and $D_{2\alpha Pan}$ receptors. The set of x, y, and z coordinates for each marker was stored by the Neurolucida program. $D_{2\alpha Pan}$ distributions in completed PD tracings were analyzed with the NeuroExplorer program.

Terminal field maps and movies

Terminal field maps were created by plotting x, y, and z values for every terminal on a given PD with SigmaPlot (Systat, San Jose, CA). In order to compare PD terminal distributions among the three preparations, the point where the dvn began (i.e., the most posterior point of the ganglion; Fig. 2A) represented zero for all three dimensions (x, y, z) in every PD neuron. Animated graphs were generated with 3D Grapher software (RomanLab, Vancouver, BC, Canada). Graphs were rotated, and frames representing different angles were exported and loaded into Windows Movie Maker Version 6 (Microsoft, Redmond, WA). Frames were assembled into movies with picture durations of 0.125 seconds and a 0.25-second transition time.

RESULTS

$D_{2\alpha Pan}$ receptors were concentrated near synapses

We previously demonstrated that DAR immunoreactivity was absent in the plasmalemma of STG neuronal somata and large-diameter neurites of the spiny lobster, *P. interruptus*; instead, DARs appeared to be concentrated in the neuropil (Clark et al., 2008). Here we further investigated $D_{2\alpha Pan}$ receptor distributions in the synaptic neuropil. Basic STG anatomy is diagramed in Figure 2A and B. Figure 2A illustrates a filled monopolar pyloric dilator (PD) neuron in a sagittal section of the STG. The single process extending from the soma, termed the primary neurite, leaves the STG and enters the dorsal ventricular nerve (dvn), at which point it is termed an axon. Prior to leaving the STG, the primary neurite branches in the neuropil, giving rise to large-diameter, secondary neurites. These, in turn, can continue to divide beyond the 16th branch order (see below), ultimately generating small-diameter processes. The large-diameter processes are in the central core of the ganglion (coarse neuropil), whereas the higher order branches reside in the fine neuropil layered between the coarse neuropil and somata (Thuma et al., 2009).

Synapses are largely restricted to the fine neuropil. EM studies have shown that synaptic contacts within the STG are found at specialized swellings along neural processes and at the terminals of fine neurites (King, 1976a,b; Kilman and Marder, 1996). As diagramed in Figure 2B, a single synaptic process contains both pre- and postsynaptic elements. The bulbous presynaptic terminal ranges from " a barely noticeable enlargement or irregularity" up to 10 μm in diameter (King, 1976a). These varicosities contain multiple (up to 18) release sites, as defined by vesicles clustered around specialized presynaptic structures known as T-bars (King, 1976a; Kilman and Marder, 1996). Extending from a presynaptic varicosity are one or more finger-like projections known as "postsynaptic twigs" (King, 1976a). Twig diameters vary from 0.25 to 1 μm, and maximal lengths are not known. Postsynaptic specializations occur on spines along or at the end of twigs (King, 1976a). Varicosities representing synaptic structures can be observed in dye-filled stomatogastric neurons with the light microscope.

Spatial relationships between D_2 receptors and presynaptic terminals were visualized in double-label IHC experiments on STG wholemounts by using antibodies against the $D_{2\alpha Pan}$ receptor (red) and synapsin (green), a protein involved in tethering presynaptic vesicles ($n = 8$). Consistent with our previous findings, $D_{2\alpha Pan}$ receptors appeared as clusters of red puncta within the fine neuropil. In some cases $D_{2\alpha Pan}$ immunoreactivity appeared to be fairly distant from presynaptic varicosities (arrowhead in Fig. 2C). Measurements in the x, y, and z directions revealed that some $D_{2\alpha Pan}$ receptors could be >10 μm from the nearest synapsin immunoreactivity, suggesting that these receptors neither resided on presynaptic terminals, nor received synaptic input. However, Figure 2C and D shows that most $D_{2\alpha Pan}$ immunoreactivity appeared to be in the vicinity of presynaptic varicosities. $D_{2\alpha Pan}$ and synapsin immunoreactivity was largely jux-

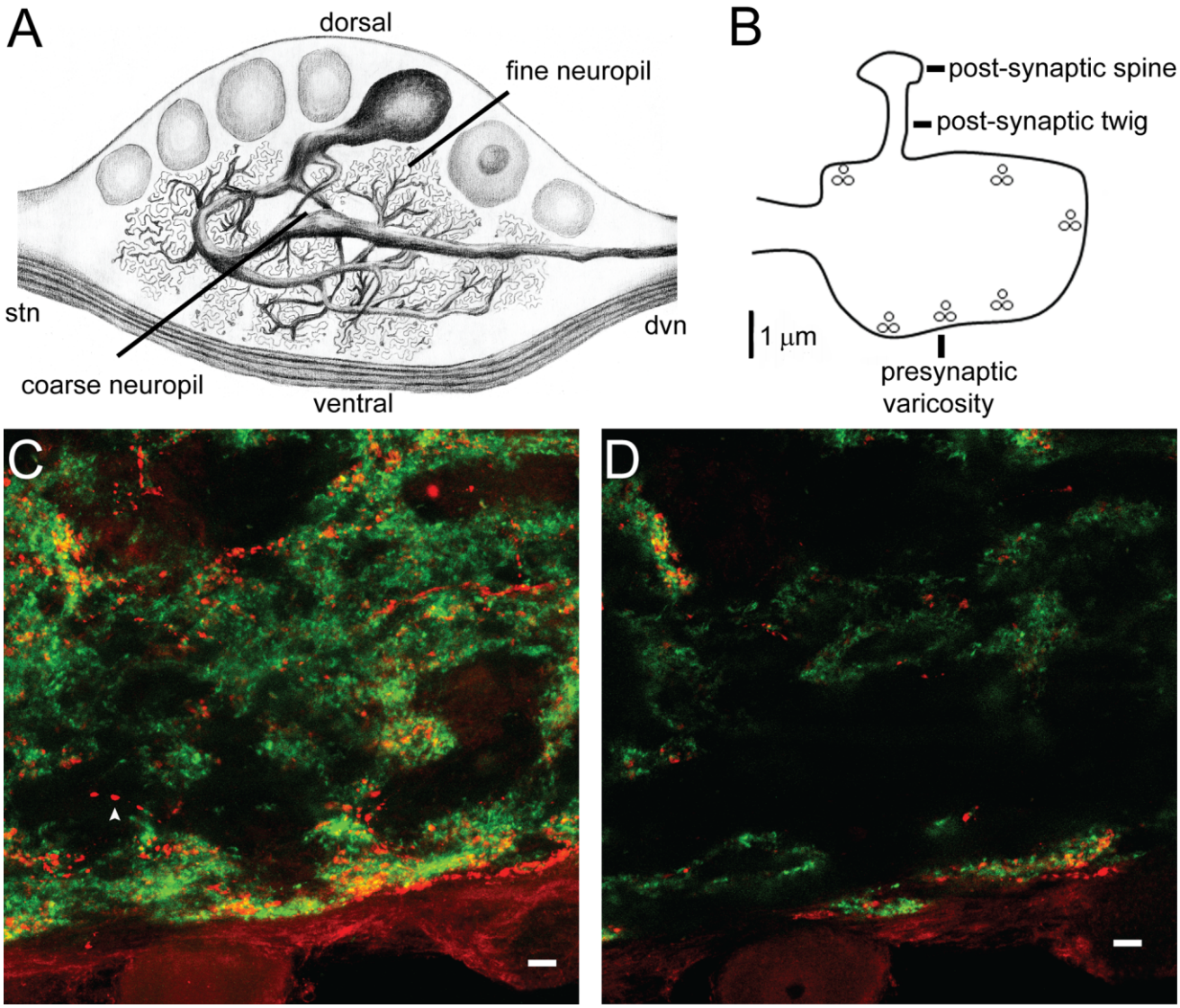

Figure 2. $D_{2\alpha Pan}$ receptors co-localize with synapsin in the fine neuropil. **A:** Illustration of a filled PD neuron in a sagittal section of the STG. A single primary process extends from the soma and exits the STG via the dvn. Before leaving the STG, the primary neurite branches to produce 9–10 large-diameter secondary neurites, that can continue to branch beyond the 16th branch order. Large-diameter neurites are found in the central, coarse neuropil. Small-diameter neurites and synapses lie in the fine neuropil. **B:** STG synaptic terminal drawn to scale. The presynaptic varicosity contains six release sites, indicated by vesicle clusters. A fingerlike postsynaptic twig extends from the presynaptic compartment and ends in a bulbous postsynaptic spine. **C,D:** A merged, 18-μm confocal projection (C) and an individual merged 1-μm optical slice (D) from a double-label IHC experiment indicate that $D_{2\alpha Pan}$ (red) and synapsin (green) can be either juxtaposed (red and green puncta) or co-localized (yellow puncta). Isolated $D_{2\alpha Pan}$ can also be observed (arrowhead). Magenta-green panels for C and D may be seen in Supplementary Figure 4. (Illustration by Sonia Hilliard, DVM.) Scale bar = 10 μm in C,D.

taposed (red and green puncta) but could also be co-localized (yellow puncta). These data suggested that $D_{2\alpha}$ receptors may reside on/near presynaptic varicosities, postsynaptic twigs/spines, and/or fine neurites in the synaptic neuropil. Similar results were obtained from double-label experiments by using antibodies against $D_{2\alpha Pan}$ receptors and synaptotagmin.

Consistent with the double-label IHC data, preliminary immunogold EM experiments indicated that surface $D_{2\alpha Pan}$ receptors were associated with varicosities containing synaptic vesicles (Fig. 3A) and fine processes/terminal swellings lacking synaptic vesicles (Fig. 3B). In most cases there appeared to be a single site of immunoreactivity on a given structure. Because receptors are known to cluster and form oligomeres (Strange, 2005; Cabello et al., 2009; Fonseca and Lambert, 2009), the single large particle could represent several receptors. In order to test the hypothesis that surface $D_{2\alpha Pan}$ receptors were

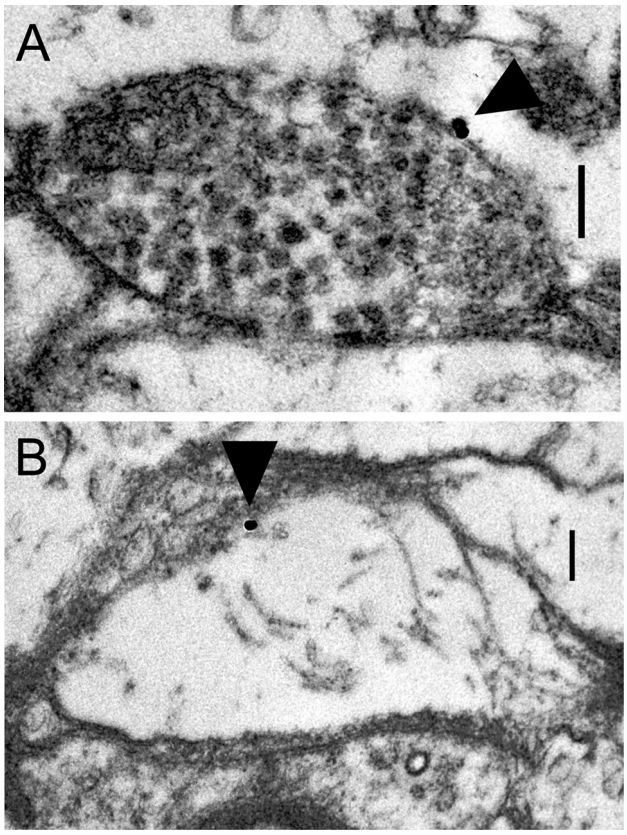

Figure 3. $D_{2\alpha Pan}$ receptors can be located on presynaptic varicosities and terminal swellings. Electron micrographs showing anti-$D_{2\alpha}$ immunogold staining (arrows) on a vesicle-containing varicosity (**A**) and a terminal swelling lacking vesicles (**B**). T-bars and postsynaptic densities indicative of synapses are not observed in these micrographs, suggesting that $D_{2\alpha Pan}$ receptors can be extrasynaptic. Scale bar = 0.25 μm in A,B.

concentrated in fine processes and presynaptic terminals, we next determined plasmalemma gold particle packing density for distinct subcellular compartments, as described in Materials and Methods. We found that the density of $D_{2\alpha Pan}$ receptors was significantly higher ($P < 0.05$) in the plasmalemma surrounding presynaptic terminals (1.97 ± 0.61 particles/μm^2) and fine neurites/terminal swellings < 1.5 μm in diameter (5.34 ± 0.97 particles/μm^2) than that surrounding processes > 1.5 μm in diameter. Absolutely no gold particles were observed in membranes of the latter profiles. Whereas receptors were concentrated near synaptic structures, they were not observed at/near synaptic release sites, defined by an obvious presynaptic T-bar and postsynaptic density; however, our EM analysis was far from exhaustive and we cannot conclude that all $D_{2\alpha Pan}$ receptors were extrasynaptic. Nevertheless, our data suggested that at least some $D_{2\alpha Pan}$ receptors might receive volume transmissions.

Dopamine transmission in the STG

We next tested the hypothesis that DA volume transmission existed in the STG by determining the spatial relationship between D_2 receptors and dopaminergic presynaptic terminals. Double-label IHC experiments with antibodies against $D_{2\alpha Pan}$ and tyrosine hydroxylase were performed on STG wholemount preparations (n = 9). Tyrosine hydroxylase, the rate-limiting enzyme in DA synthesis, is distributed throughout the cytosol of dopaminergic terminals in mammals and crustaceans (Pulver et al., 2003; Mengual and Pickel, 2004).

Consistent with previous work on the spiny lobster (Barker et al., 1979), we observed approximately two to eight tyrosine hydroxylase-containing projection fibers in the stn. It was not clear how many of these fibers were due to branching within the stn. Tyrosine hydroxylase was also observed in projection neuron terminals within the STG; however, resident STG neurons did not contain tyrosine hydroxylase. Green puncta representing tyrosine hydroxylase immunoreactivity were limited to the fine neuropil, and were not observed in the core of the STG. Figure 4 shows the relationship between D_2 receptors (red) and dopaminergic terminals (green) within the STG neuropil. $D_{2\alpha Pan}$ and tyrosine hydroxylase immunoreactivity usually appeared in the same vicinity, but yellow pixels were almost never observed. In agreement with our EM study, these data suggested that classical synapses, in which pre- and postsynaptic terminals are separated by a 16-nm cleft (King, 1976a), were largely absent between $D_{2\alpha Pan}$ and tyrosine hydroxylase-containing terminals. However, tyrosine hydroxylase-containing varicosities appeared to be close enough to release DA to $D_{2\alpha Pan}$ receptors in a paracrine fashion.

PD neurons expressed D_2 but not D_1 receptors

We next explored DA receptor distributions at the level of single identified neurons. In the spiny lobster, DA acts directly on the two PD neurons to reduce their excitability and output through a variety of mechanisms (Flamm and Harris-Warrick, 1986a,b; Johnson and Harris-Warrick, 1990; Johnson et al., 1993; Kloppenburg et al., 1999; Kloppenburg et al., 2000). There are three known DARs that could potentially mediate DA-induced changes in PD neurons: $D_{1\alpha Pan}$, $D_{1\beta Pan}$, and $D_{2\alpha Pan}$. We previously found that all of these receptors were expressed in the STG, and each coupled with distinct signaling cascades (Clark et al., 2008). Here we used single cell RT-PCR to determine which DA receptor transcripts were expressed in PD neurons. After electrophysiologically identifying a PD neuron, the cell was removed from the ganglion either with or without the cap of glial cells ensheathing the soma. Each cell was then tested for the presence of $D_{1\alpha Pan}$, $D_{1\beta Pan}$, $D_{2\alpha Pan}$, and α-tubulin transcripts. PD neurons with glial caps all

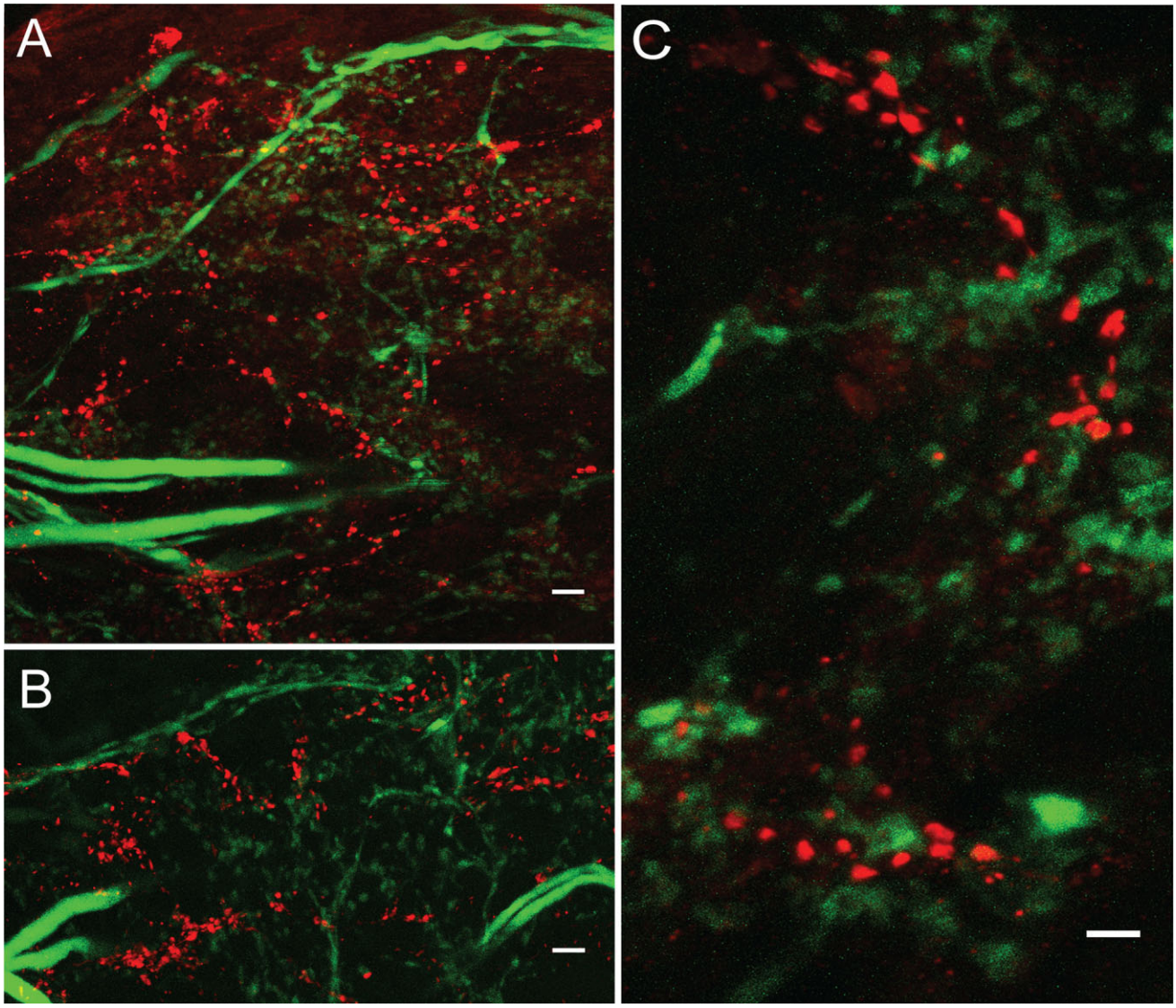

Figure 4. $D_{2\alpha Pan}$ receptors appear to receive volume transmissions. Three double-label IHC experiments showing that $D_{2\alpha Pan}$ receptors (red) and tyrosine hydroxylase-containing terminals (green) are not arranged in classical point-to-point synapses. Merged 23-μm (**A**) and 40-μm (**B**) confocal projections from the synaptic neuropil showing that clusters of red puncta are associated with green puncta. **C:** High-magnification 16-μm merged confocal projection showing a lack of co-localization (yellow) and that red and green puncta are not in a 1:1 relationship. Magenta-green panels may be seen in Supplementary Figure 5. Scale bar = 10 μm in A,B; 5 μm in C.

expressed $D_{1\beta Pan}$, $D_{2\alpha Pan}$, and α-tubulin transcripts (n = 8), whereas a subset of cells (two of eight) also expressed $D_{1\alpha Pan}$ transcripts (Fig. 5A). In PD neurons that were isolated without glial caps (n = 5), only $D_{2\alpha Pan}$ and α-tubulin transcripts were detected (Fig. 5B).

In order to determine whether protein distributions in the PD were consistent with the single cell RT-PCR studies, we performed IHC experiments on STG wholemount preparations containing dye-filled PD neurons. Whereas there are two PD neurons in an STG, only one of the two was filled in these studies. Consistent with the single cell RT-PCR studies, anti-$D_{2\alpha}$ produced robust staining in PD neurons (Fig. 6, n = 11). In contrast, we observed no $D_{1\alpha Pan}$ (n = 3) or $D_{1\beta Pan}$ (n = 6) immunoreactivity in PD neurons, although receptor immunoreactivity was observed in other unfilled neurons. Additionally, sparse and patchy D_1 immunoreactivity was sometimes observed around a PD soma. Together, the single cell RT-PCR and IHC data suggest that PD neurons exclusively express D_2 receptors, whereas some glial cells surrounding the PD soma may express D_1 receptors.

$D_{2\alpha Pan}$ distributions in the PD somatodendritic compartment

PD neurons are geometrically complex (Fig. 2A), and $D_{2\alpha Pan}$ receptors could reside in any of several distinct compartments. We examined the subcellular distribution

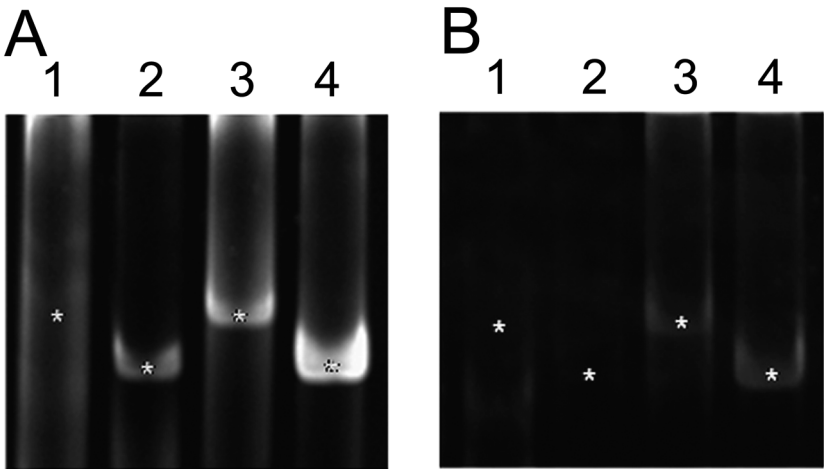

Figure 5. PD neurons express D_2 but not D_1 receptors. Individual PD neurons, physically isolated with (**A**) versus without (**B**) their glial caps, served as templates in RT-PCRs. PCR products were visualized on ethidium bromide-stained polyacrylamide gels. The RT-PCRs tested each PD neuron for the expression of four transcripts: $D_{1\alpha Pan}$, lane 1; $D_{1\beta Pan}$, lane 2; $D_{2\alpha Pan}$, lane 3; and α-tubulin, lane 4. The expected sizes of the PCR products are indicated with asterisks.

of the $D_{2\alpha Pan}$ receptors within the multipart somatodendritic compartment of dye-filled PD neurons from wholemount anti-$D_{2\alpha}$ IHC preparations. Careful examination of a complete series of 1-μm optical sections through a given PD neuron suggested that $D_{2\alpha Pan}$ receptors were located in terminals and/or varicosities of fine neurites. Receptors were not observed in the plasma membrane of the soma or higher order branches, rather, $D_{2\alpha Pan}$ immunoreactivity was localized to endomembrane structures within these compartments (Fig. 6A). Although $D_{2\alpha Pan}$ immunoreactivity was obvious in the initial segment of the primary neurite (Fig. 6B), it tapered off after the final secondary branch and did not continue to the start of the dvn. Receptors appeared to be transported to some, but not all higher order neurites (Fig. 6B). $D_{2\alpha Pan}$ immunoreactivity was also observed in smaller diameter neurites and varicosities (Fig. 6B,C). At the highest magnification some varicosities and fine processes appeared to contain $D_{2\alpha Pan}$ receptors in their plasmalemma, as evidenced by the absence of a red cytoplasmic ring surrounding the $D_{2\alpha Pan}$ immunoreactivity in confocal projections (Fig. 6D). Whereas we occasionally discerned individual putative synaptic processes containing both pre-and postsynaptic elements (e.g., compare underlined structure in Fig. 6D with Fig. 2B), it was usually impossible to determine whether $D_{2\alpha Pan}$ receptors were in pre- and/or postsynaptic varicosities with the light microscope.

Dopamine receptors were not observed in the PD axonal compartment

Figure 1A illustrates PD axonal projections. Whereas the somatodendritic compartments of the two PD neurons lie within the STG, the PD axons project out the dvn, whereupon, they branch and send one branch through each of

Figure 6. The $D_{2\alpha Pan}$ receptor is restricted to the PD somatodendritic compartment. **A:** Merged 1-μm optical section from a wholemount anti-$D_{2\alpha}$ (green) IHC preparation containing a Texas red-filled PD neuron. Yellow staining indicates $D_{2\alpha Pan}$ receptor expression in the PD soma and primary neurite. **B:** A 34-μm merged confocal projection showing the same PD neuron as in A branching throughout the STG neuropil. $D2_{\alpha Pan}$ receptors are in cytoplasmic transport vesicles in the primary neurite (labeled A), and some higher order neurites. Arrows indicate higher order neurites lacking the receptor. Arrowheads show $D_{2\alpha Pan}$ receptors in PD terminals. The green channel was set to maximum intensity for this panel in order to detect receptors in the finest neurites. At lower intensity, vesicles in the primary neurite showed a punctuate distribution, as in A. **C:** A 29-μm merged confocal projection from deep within the synaptic neuropil showing a single tertiary and higher order neurites. Arrowheads show $D_{2\alpha Pan}$ receptors in PD putative synaptic terminals. Green staining represents $D_{2\alpha Pan}$ receptors in unidentified neurons. **D:** High-magnification 4-μm projection from the synaptic neuropil showing a cluster of PD terminals, some of which contain $D_{2\alpha Pan}$ receptors. A putative synaptic structure containing both pre- and postsynaptic elements, as illustrated in Figure 2B, is underlined in white. Note that the two postsynaptic twigs end in bulbous structures, consistent with previously described postsynaptic spines (King, 1976a). Also note that the ridge of green observed on some putative synaptic processes does not represent a technical artifact (i.e., red-green channel offset), and is consistent with the fact that the antibody recognizes an extracellular N-terminal epitope. **E:** Montage of confocal projections showing only background levels of anti-$D_{2\alpha}$ immunoreactivity in/along the PD axon as it leaves the STG and projects down the dvn. **F:** An unmerged 1-μm confocal slice showing PD NMJs. The presence of synapsin (red) and the absence of $D_{2\alpha Pan}$ receptor (green) staining indicates that there are no detectable $D_{2\alpha Pan}$ receptors in PD axon terminals. A magenta-green version may be seen in Supplementary Figure 6. Scale bar = 20 μm in A; 10 μm in B,C; 2 μm in D; 50 μm in E; 5 μm in F.

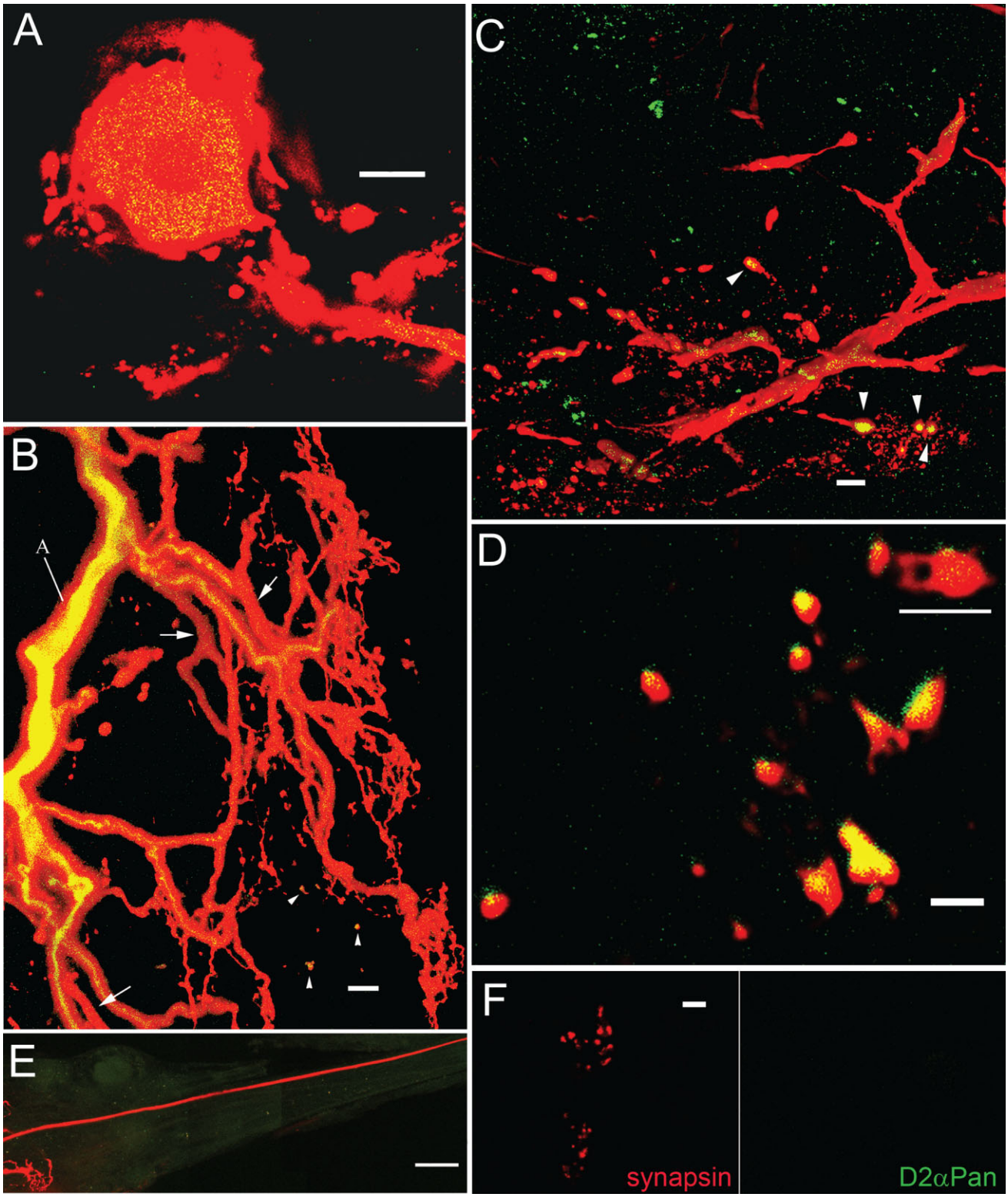

Figure 6

the two lateral ventricular nerves (lvn) and finally into the PD nerves (pdn) before innervating the PD muscles. It was previously demonstrated that DA could modulate the axonal compartment of PD neurons in the American lobster, *H. americanus*, and that receptors appeared to reside in the dvn and pdn (Bucher et al., 2003). We asked whether $D_{2\alpha Pan}$ receptors were located in these axonal compartments of PD neurons in the spiny lobster, *P. interruptus*, by

using dye-filled PD neurons from anti-$D_{2\alpha}$ IHC wholemount experiments. D_2 receptors were not observed in PD axonal compartments as they traversed the dvn (Fig. 6E, n = 5). We could not observe PD axons in the lvn, as the dye did not diffuse beyond the dvn-lvn branch point. Unlike the dvn and lvn, which contain axons from many cell types, the pdn only contains the two PD axons. $D_{2\alpha Pan}$ receptors were not observed in axonal membranes in the pdn (n = 5).We also examined $D_{2\alpha Pan}$ receptor distribution in PD axon terminals at the NMJ. Double-label experiments with anti-$D_{2\alpha}$ and anti-synapsin antibodies showed no receptor immunoreactivity at the PD NMJ, although anti-synapsin immunoreactivity was observed (Fig. 6F, n = 7). In sum, PD neurons expressed detectable levels of $D_{2\alpha Pan}$ receptors in their somatodendritic compartments, but anti-$D_{2\alpha}$ immunoreactivity was not above background levels in axonal compartments.

Mapping $D_{2\alpha Pan}$ receptors onto 3D renderings of PD neurons suggests specific targeting

Whereas our data suggested that PD D_2 receptors were restricted to the somatodendritic compartment, they did not reveal whether receptors were explicitly targeted within this compartment. To test the hypothesis that D_2 receptors can be restricted to a specific subset of varicosities in a given cell type, we carefully mapped $D_{2\alpha Pan}$ distribution within the somatodendritic compartment of each of three PD neurons. Anti-$D_{2\alpha}$ IHC experiments were performed on STG wholemount preparations containing a single dye-filled PD neuron. Confocal stacks representing one entire PD neuron were imported into a software program that enabled us to trace the filled neuron manually (see Materials and Methods). The trace was then used to render a 3D model of the neuronal somatodendritic compartment, and the presence or absence of $D_{2\alpha Pan}$ receptors in each neurite and varicosity was marked.

Figure 7 and Supplementary Figure S2 show 2D representations of the somatodendritic compartment for the three traced PD neurons. Consistent with a previous report (Thuma et al., 2009), the length and trajectory of the primary neurite varied, possibly due to different soma locations (e.g., anterior vs. middle vs. posterior region of the STG) and the need for the primary process to extend throughout the neuropil. Each PD neuron had 9–10 secondary branches arising from the primary neurite. We designated a secondary branch, and all branches stemming from it, as a secondary branch cluster. Each secondary branch cluster is shown in a different color, with the color indicating the order in which the secondary branched from the primary neurite. A comparison of each secondary branch cluster across the three PD neurons is shown in Figure 8.

There was substantial variability in the higher order branching pattern across the three PD neurons (Fig. 8). A similar finding was previously reported for all STG cell types in two lobster species (Bucher et al., 2007; Thuma et al., 2009). A given secondary branch cluster showed extensive arborization extending up to or beyond the 13th branch order (Thuma et al., 2009). As previously described for STG neurons in *H. americanus* (Bucher et al., 2007), we observed a diversity of diameter changes at branch points, such that the diameter of the daughter branch could be smaller, larger, or the same as the mother branch. In order to generate terminal field maps of secondary branch clusters, every terminal for each secondary branch cluster on a given PD was graphed as a colored structure in 3D space in which the color corresponded to that of the secondary branch cluster in Figures 7 and 8. The scatter plots in Figure 9 and Supplementary Figure S3 show that the terminal fields of the secondary branch clusters were largely non-overlapping and that a given secondary branch cluster occupied a different sector of the STG in each animal (e.g., the region occupied by the yellow structures in Suppl. Fig. S3 varied for each animal). Wilensky et al. (2003) reported a similar finding for the VD neuron in the crab, *Cancer borealis*.

Whereas higher order branching patterns were variable, the number of varicosities per branch order was fairly consistent (Table 3). As branches were traced, varicosities were marked with pale blue circles (Fig. 8). Varicosities appeared along neurites that continued to arborize, but in most cases, were at or near a terminal. Whereas varicosities were found on all branch orders with the exception of the primary neurite, the number of varicosities per branch increased with increasing branch order (Table 3). In some cases, a single neurite contained multiple varicosities, which were most often clustered in one region of the branch. Our data also showed that only 60 ± 6% of the terminals possessed varicosities (n = 3, Table 4).

$D_{2\alpha Pan}$ receptor distributions were mapped onto the traced neurons. Markers were placed to indicate the presence (orange triangles, Fig. 8) or absence (red crosses, Fig. 8) of $D_{2\alpha Pan}$ immunoreactivity within each branch and varicosity. Our markers did not discriminate between $D_{2\alpha Pan}$ staining in the cytoplasm versus the membrane. In all cases, $D_{2\alpha Pan}$ immunoreactivity in a daughter branch was preceded by staining in the mother branch. Taken together, these data generated several important findings.

First, the data showed that the percent of $D_{2\alpha Pan}$-containing varicosities was similar across PD neurons, and on average, 40 ± 3% of the varicosities in any given PD neuron contained $D_{2\alpha Pan}$ receptors (n = 3). These data are consistent with previous Ca^{2+} imaging and electrophysiological studies, which showed that DA modulated the Ca^{2+} current in a subset of PD varicosities (Kloppenburg et al., 2000, 2007). Nevertheless, in order to show that the observed staining pattern was not an artifact of poor antibody

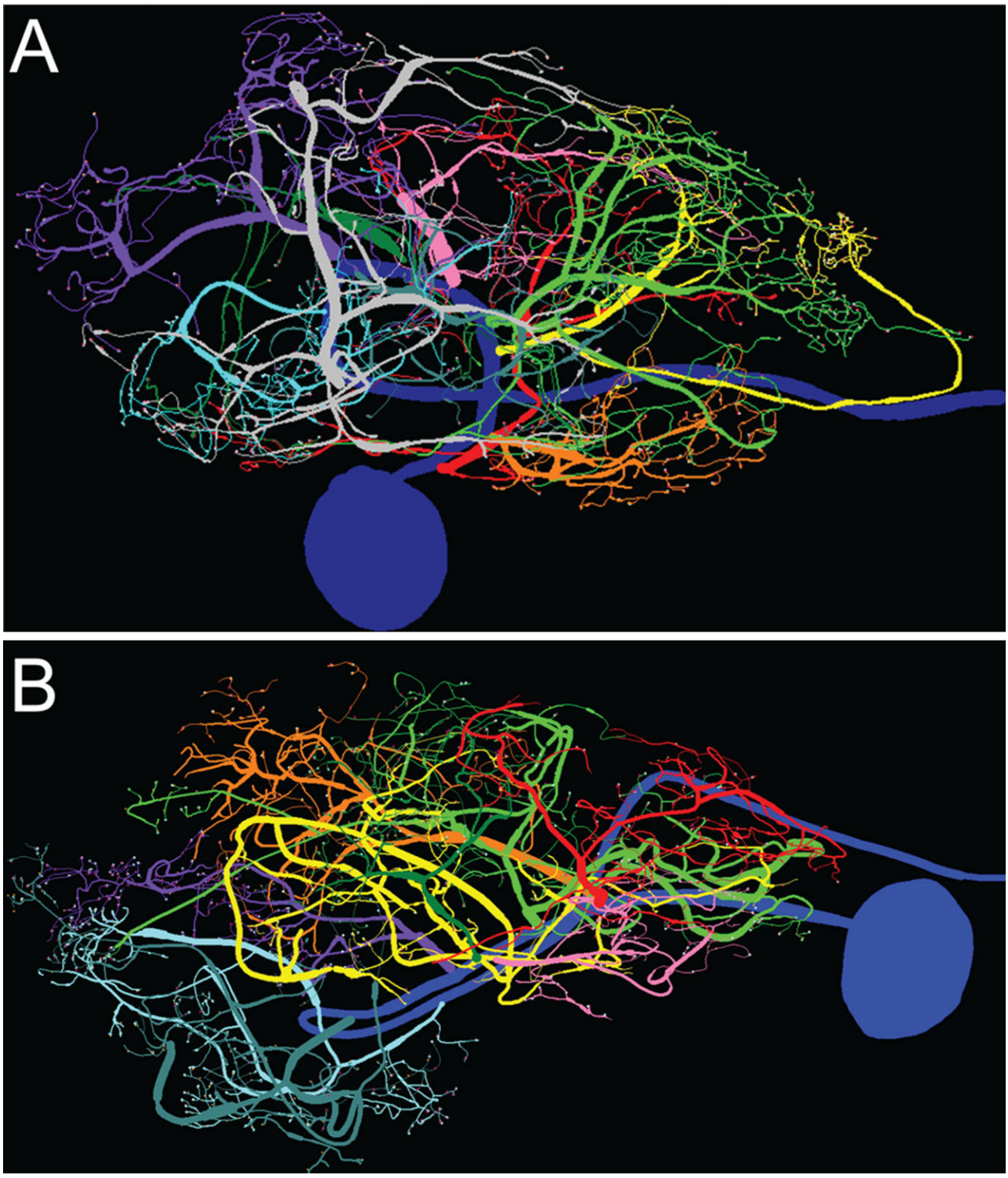

Figure 7. PD neurons from two different animals. 3D renderings of PD 1 (**A**) and PD2 (**B**) neurons are displayed in 2D. Secondary branch clusters are color coded according to order of emergence from the primary neurite: red-orange-yellow-light green-pink-dark green-light purple-teal-cyan-gray. In all panels: left = anterior, right = posterior. Varicosities are marked with pale blue circles, and $D_{2\alpha Pan}$ receptors in varicosities are marked by orange triangles.

penetration, we repeated the IHC experiments on sectioned STGs, as described in Materials and Methods. The logic was that penetration should not be an issue in these thinner slices. $D_{2\alpha Pan}$-containing varicosities, as well as the total number of varicosities were counted for all sections of a given ganglia. We observed that 43 ± 6% of the

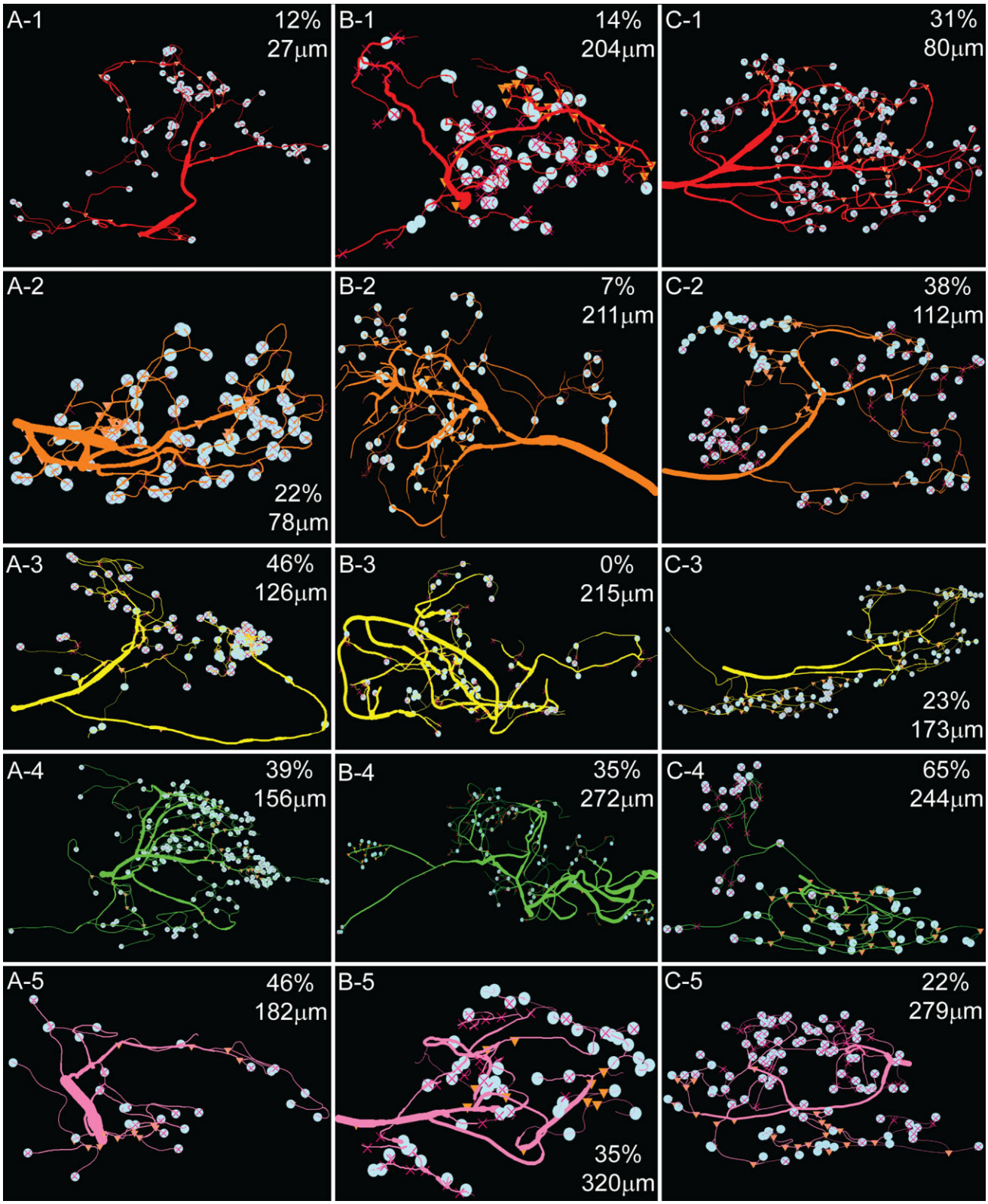

Figure 8. **A1–C5:** $D_{2\alpha Pan}$ receptor distribution in PD neurites and varicosities. Secondary branch clusters for the three PD neurons are displayed according to order of emergence, where branch 1 is closest to the soma. The point of emergence from the primary neurite is shown in microns in the right corner of each panel, where 0 μm is the point where the primary neurite emerges from the soma. Varicosities are marked by pale blue circles. The percent of varicosities containing $D_{2\alpha Pan}$ receptors is also listed in the right corner of each panel. ▲ = marker for $D_{2\alpha Pan}$ immunostaining in neurite/varicosity; X = marker for absence of $D_{2\alpha Pan}$ immunostaining in branch or varicosity. Note that some markers may not be visible, as they are behind the pale blue circle.

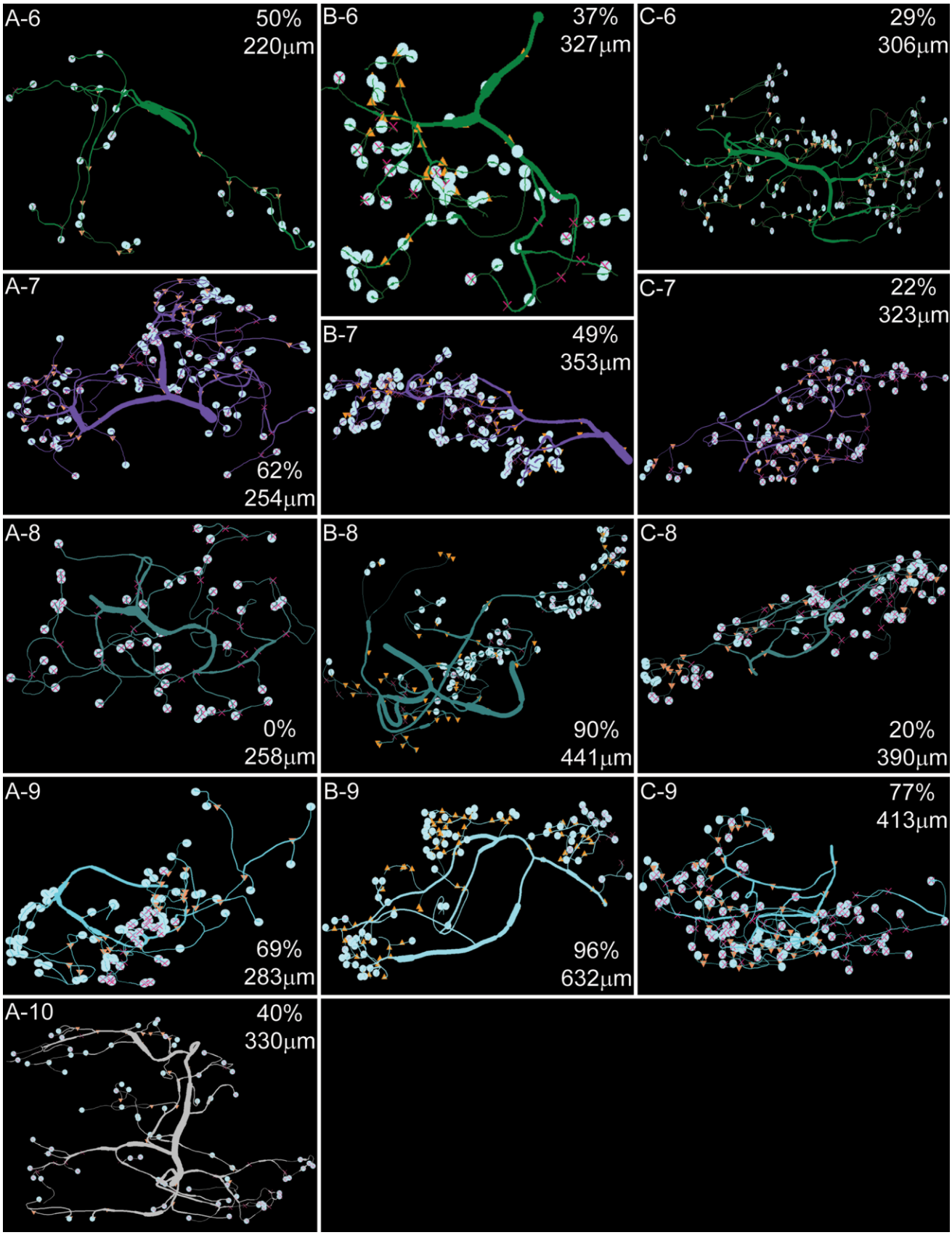

Figure 8 (Continued)

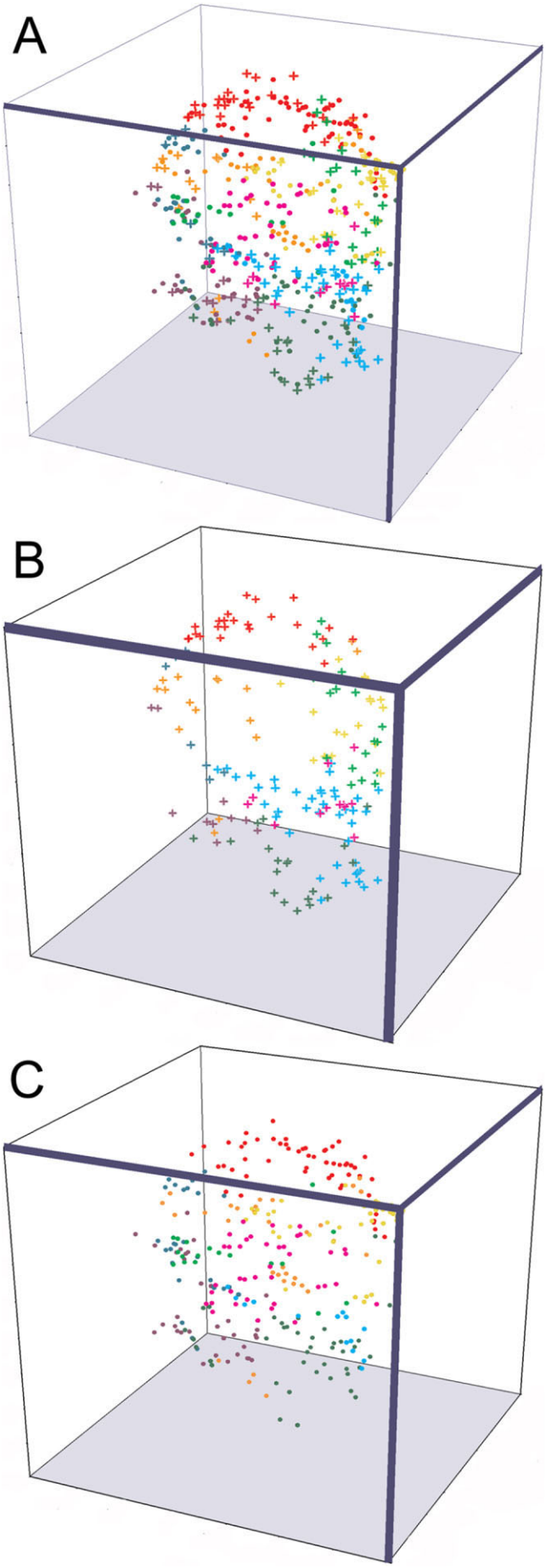

varicosities contained $D_{2\alpha Pan}$ receptors in the sectioned ganglia, and there was no staining in the membrane of the soma or large-diameter processes. These data suggested that the lack of $D_{2\alpha Pan}$ immunoreactivity in ~60% of the varicosities was not due to poor antibody penetration.

Second, the data revealed a very interesting receptor distribution pattern (Fig. 9, Suppl. Fig. S3, and Supplementary Movie). Namely, the terminals containing $D_{2\alpha Pan}$ receptors formed a patchy, hollow shell that encapsulated the terminals lacking D_2 receptors. In other words, terminals containing $D_{2\alpha Pan}$ receptors were largely on the periphery of the fine neuropil, whereas terminals lacking $D_{2\alpha Pan}$ receptors were distributed throughout the fine neuropil, but were usually deeper than $D_{2\alpha Pan}$-containing terminals along the same radius. Here we again emphasize that the distribution pattern is not due to poor antibody penetration into the center of wholemount preparations, as the same staining pattern was observed in wholemounts and sectioned ganglia (see above) and $D_{2\alpha Pan}$ receptors were observed in the central coarse neuropil, as they were transported down the large-diameter neurites (Fig. 6).

Third, $D_{2\alpha Pan}$ receptors were not uniformly distributed among secondary branch clusters. That is to say, it was not the case that 40% of the terminals on every secondary branch cluster contained $D_{2\alpha Pan}$ receptors. Instead, one secondary branch cluster could contain D_2 receptors in nearly all of its varicosities, whereas another could be completely devoid of $D_{2\alpha Pan}$ receptors, and each PD neuron examined had one extended cluster of neurites lacking $D_{2\alpha Pan}$ receptors. For example, PD2, cyan cluster 9 (Fig. 8, B-9) contained $D_{2\alpha Pan}$ receptors in 96% of its varicosities, whereas yellow cluster 3 (Fig. 8, B-3) completely lacked $D_{2\alpha Pan}$ in all varicosities. PD1 teal cluster 8 was also devoid of $D_{2\alpha Pan}$ receptors (Fig. 8, A-8). Furthermore, PD3 pink cluster 5 immediately split into two tertiary processes, and $D_{2\alpha Pan}$ receptors were associated with only one of the two

Figure 9. PD terminals are largely non-overlapping and restricted within the STG. Dendritic terminals are represented as colored objects. The 3D position of every terminal on a PD neuron (PD3) was plotted in 3D space relative to the origin of the dvn. All terminals from a given secondary branch cluster share the same color, which corresponds to the color of the secondary branch clusters shown in Figures 7 and 8. Filled circles and crosses represent terminals bearing and lacking $D_{2\alpha Pan}$ receptors, respectively. The terminal field maps contain either (A) all terminals, (B) only terminals bearing $D_{2\alpha Pan}$ receptors or (C) only terminals lacking $D_{2\alpha Pan}$ receptors. As shown in the Supplemental Movie, when the plots were continuously rotated about all axes by using3D Grapher software, it became clear that the terminals containing $D_{2\alpha Pan}$ receptors (B) formed a patchy, hollow shell that encapsulated the terminals lacking D_2 receptors (C).

TABLE 3.
Average Values for Three Pyloric Dilator (PD) Neurons

Branch order	Mean no. of branches (n = 3)	Mean % of branches with $D_{2\alpha Pan}$ (n = 3)	Mean no. of varicosities per branch (n = 3)	% of varicosities with $D_{2\alpha Pan}$ (n = 3)
2	9 ± 0.3	97 ± 3	0.04 ± 0.04	33 ± 33
3	24 ± 3.9	79 ± 5	0.25 ± 0.10	75 ± 13
4	56 ± 7.2	65 ± 5	0.48 ± 0.18	54 ± 12
5	110 ± 7.4	55 ± 5	0.52 ± 0.15	44 ± 4
6	175 ± 17.7	45 ± 5	0.64 ± 0.06	42 ± 2
7	211 ± 21.0	42 ± 5	0.65 ± 0.06	38 ± 5
8	195 ± 33.0	37 ± 5	0.67 ± 0.03	40 ± 3
9	162 ± 35.4	40 ± 4	0.67 ± 0.06	35 ± 3
10	113 ± 19.5	32 ± 4	0.71 ± 0.10	34 ± 4
11	61 ± 6.2	32 ± 8	0.80 ± 0.01	43 ± 12
12	32 ± 4.9	25 ± 11	0.79 ± 0.07	24 ± 7
13	16 ± 0.3	58 ± 17	0.96 ± 0.05	43 ± 11
14	10[1]	40[1]	0.95	38[1]
15	4[1]	50[1]	0.75	67[1]
16	3[1]	100[1]	1.0	100[1]

[1]Values are exclusively from PD-1, as PD-2 and PD-3 did not have branches above the 13th order.

TABLE 4.
$D_{2\alpha Pan}$ Receptor Distribution in Pyloric Dilator (PD) Neuron Terminals

	Total no. of terminals	Terminals with varicosities		Terminals lacking varicosities	
		+ $D_{2\alpha Pan}$	− $D_{2\alpha Pan}$	+ $D_{2\alpha Pan}$	− $D_{2\alpha Pan}$
PD-1	312	54	95	59	104
PD-2	304	90	111	36	67
PD-3	461	186	92	123	60

branches (Fig. 8, C-5). The only obvious difference between secondary branch clusters containing versus lacking $D_{2\alpha Pan}$ receptors was their point of emergence from the primary process. The average distance between two secondary branch points along a primary neurite was 42.6 ± 7.6 μm, but the secondary branches lacking $D_{2\alpha Pan}$ receptors emerged ≤4 μm after the preceding branch.

In general, the distance from the preceding or following branch along the primary neurite did not correlate with the percentage of D_2-containing varicosities in a secondary branch cluster (linear regressions returned an average $R^2 = 0.096$ and 0.177, respectively, n = 3). When $D_{2\alpha Pan}$ receptors were present in a secondary branch cluster, they were not evenly dispersed throughout the cluster, but segregated with increasing branch order. For example, $D_{2\alpha Pan}$ receptors were observed on 14% of the varicosities in the PD2 red cluster 1 (Fig. 8). The receptors were not distributed among both tertiary branches, but segregated to one. The receptors continued to segregate to one or a few branches with each increasing branch order.

Fourth, $D_{2\alpha Pan}$ receptors were found on terminals lacking varicosities. Table 4 indicates that on average a PD neuron contained 359 ± 51 terminals, and of those, approximately 209 ± 38 contained varicosities (n = 3). Note that the number of terminals and varicosities is underestimated, as the entire volume of a neuron was not traced (Table 2) and the number of varicosities per neurite increased with branch order (Table 3). $D_{2\alpha Pan}$ receptors were not exclusively associated with varicosities. Thus, $D_{2\alpha Pan}$ receptors were found in 46 ± 10% and 49 ± 9% of the terminals lacking versus bearing varicosities, respectively (n = 3). Here it must be noted that not all terminals corresponded to the end of a neurite, but represented the point at which a neurite could no longer be accurately traced. Thus, immunostaining in terminals lacking varicosities could represent receptors that were being trafficked to finer neurites bearing varicosities.

In sum, the PD terminals containing $D_{2\alpha Pan}$ receptors formed a patchy shell around the perimeter of the neuropil. Approximately 40% of the total number of varicosities in each PD neuron contained $D_{2\alpha Pan}$ receptors. Receptors were usually restricted to a subset of neurites on a given secondary branch cluster, although in some cases a secondary branch cluster could completely lack $D_{2\alpha Pan}$ receptors or contain them at nearly all varicosities.

DISCUSSION

In order to evaluate which aspects of DAR function evolve with cell types or circuits, we first defined DA transmission and receptor distributions for an identified neuron located in the STG of the spiny lobster, *P. interruptus*. We found that PD neurons expressed D_2, but not D_1 receptors. $D_{2\alpha Pan}$ receptors appeared to receive mainly volume transmissions. Surface $D_{2\alpha Pan}$ receptors were not observed in the soma, neurites, or axon, but were explicitly targeted to approximately 40% of the total number of synaptic processes, and were not evenly dispersed among all neurites.

As described below, with this information in hand, we could perform a comparison of D_2 receptor function in two neurons from vastly different systems: lobster PD neurons receiving inhibitory input versus mammalian striatal MSNs receiving excitatory input. The latter have been extensively studied and recently reviewed (Kauer and Malenka, 2007; Schultz, 2007; Surmeier et al., 2007; Kreitzer and Malenka, 2008; Yao et al., 2008). Our comparison suggests that receptors may be differentially targeted in each cell type to bring about the same end: a reduction in neuronal output.

D_2 receptor distribution patterns in the PD neuron

G protein-coupled receptors exist in multiprotein complexes designed to produce signals that can be highly localized and restricted to within 1 μm of the complex (Zaccolo and Pozzan, 2002) or show varying degrees of global spread (Nikolaev et al., 2006). Receptor function is therefore partially dictated by the complex within which it resides, and for those receptors generating restricted signals, by the compartmentalization of the receptor complex. Here we defined PD $D_{2\alpha Pan}$ receptor distributions in wholemount IHC experiments by using confocal and electron microscopy. The usual caveats apply: Because arthropod D_2 transcripts are extensively alternately spliced (Hearn et al., 2002), and DARs can reside in different types of multiprotein complexes that alter receptor clustering and conformations, our antibody may only recognize a subset of isoforms in a subset of complexes; and hence, only those receptors performing a subset of functions.

PD $D_{2\alpha Pan}$ receptors were concentrated at synaptic processes. PD synaptic processes are complex structures containing both pre- and postsynaptic elements. In only rare instances did our confocal experiments capture both the pre-and postsynaptic varicosities of a single synaptic structure (Fig. 6D). In these cases, pre-and postsynaptic varicosities appeared to be separated by ≤ 1 μm. Because our 3D models were built from 1-μm serial sections, it is likely that a single varicosity in our model neurons represents both pre- and postsynaptic elements. On the other hand, preliminary immunogold EM experiments revealed $D_{2\alpha Pan}$ receptors in presynaptic varicosities and in terminal swellings lacking vesicles. It is not clear whether the latter represent postsynaptic twigs/spines and/or neurite terminals lacking chemical synapses.

Electrophysiological data suggest that MSNs may target DARs to specific inputs (Goto and Grace, 2005). In support of the idea that neurons can direct $D_{2\alpha Pan}$ receptors to a subset of synaptic structures, we found that approximately 40% of the total number of varicosities in any given PD neuron contained $D_{2\alpha Pan}$ receptors. These data are consistent with calcium imaging studies showing that DA inhibited a depolarization-evoked increase in Ca^{2+} in approximately 50% of PD varicosities containing voltage-gated calcium channels (Kloppenburg et al., 2000, 2007). Whereas our data support the idea that receptors can be restricted to synapses involving specific inputs or outputs, it is also possible that $D_{2\alpha Pan}$ receptors may be present at all synapses, but distributed to only 40% of the individual contact sites comprising a given synapse. It has been suggested that this may prevent overmodulation of a neuron (Kloppenburg et al., 2007).

It is intriguing that for each PD neuron, an extended cluster of neurites (e.g., an entire secondary branch cluster) was devoid of $D_{2\alpha Pan}$ receptors. The functional significance and mechanism(s) underpinning this phenomenon are unclear. These branch clusters have average numbers of terminals and varicosities, and do not appear to be structurally distinct, except that each emerged almost immediately after the preceding branch. It is not clear what, if any, role this played in inhibiting receptor trafficking, or whether other neuromodulatory receptors (e.g., octopamine or peptide receptors) can be localized to these branch clusters.

$D_{2\alpha Pan}$ receptors formed a patchy shell around the neuropil. This may correspond to the pattern of modulatory innervation or may function to increase access to neurohormones (Thuma et al., 2009). D_2 receptor trafficking is poorly understood (Bockaert et al., 2004; Kabbani and Levenson, 2007; Yao et al., 2008), but it has been shown that agonist application may stimulate general D_2 receptor trafficking throughout the cell (Tirotta et al., 2008). However, somewhat surprisingly, in at least some cases it appears that fast synaptic (e.g., glutamatergic), rather than neuromodulatory (e.g., dopaminergic) input, ultimately determines modulatory receptor distributions (Sun et al., 1996).

D_2 receptors receive volume transmissions in the STG and striatum

Consistent with their modulatory role, D_2 receptors appear to receive slow, nonspecific, energy-efficient volume transmissions in both the striatum and STG. Greater than 95% of striatal D_2 receptors receive volume transmissions, whereby DA diffuses out of an open synapse to bind to extrasynaptic receptors within an approximately 12-μm radius (Zoli et al., 1998). STG $D_{2\alpha Pan}$ receptors also appeared to mainly receive volume transmissions. Red-tagged $D_{2\alpha Pan}$ receptors and green-tagged tyrosine hydroxylase-containing presynaptic terminals were seldom in close enough proximity to appear yellow in merged confocal slices, as would be expected for pre- and postsynaptic structures separated by a 16-nm cleft, nor was there a 1:1 ratio between red and green puncta in the IHC experiments. Moreover, although our studies were not exten-

sive, $D_{2\alpha Pan}$ receptors were not observed opposite a presynaptic release site in electron micrographs.

D_2 receptor affinities for DA may not be conserved across species. Both the striatum and STG receive dopaminergic input from modulatory projection neurons. Tonically firing midbrain DA neurons maintain nM concentrations of extracellular DA in the striatum, which activates high-affinity D_2 receptors (Goto et al., 2007). PD neurons may also be continuously exposed to nM concentrations of DA, as the STG resides in a blood vessel and is constantly bathed by hemolymph containing DA (Sullivan et al., 1977). The extent to which $D_{2\alpha Pan}$ receptors are activated by neurohormonal DA and/or dopaminergic projection neurons is not clear. Electrophysiological experiments suggested that the threshold concentration of DA required to reduce spike frequency significantly in a synaptically isolated PD neuron was $\sim 10^{-6}$ M (Flamm and Harris-Warrick, 1986b). When expressed in HEK cells, the affinity of $D_{2\alpha Pan}$ receptors for DA varied according to splice form, with the most sensitive isoform having an EC_{50} of $\sim 10^{-8}$ M (Clark and Baro, 2007). Affinities in the native system have not been determined, nor have all isoforms been isolated. It is noteworthy that the human and fruit fly D_2 receptor EC_{50}s for DA were not significantly different when tested in parallel luciferase assays (Hearn et al., 2002).

D_2 transduction cascades in PD versus striatal MSNs

D_2 receptor transduction cascades appear to be similar in the striatum and STG. DA application acutely increases voltage-dependent outward currents, such as the transient potassium current (I_A), and reduces Ca^{2+} currents (I_{Ca}) in PD and D_2-containing striatal MSNs (Kloppenburg et al., 1999, 2000, 2007; Nicola et al., 2000; Surmeier et al., 2007). Both arthropod and mammalian D_2 receptors can couple with Gi/o, and acute D_2 modulation of voltage-dependent ionic currents is achieved through a variety of Gi/o signaling cascades. In MSNs, D_2 modulates I_A via $G\alpha_{i/o}$ subunits that decrease adenylyl cyclase to reduce cAMP and inhibit protein kinase A (PKA) activity (Perez et al., 2006). MSN D_2 reduces I_{Ca} by coupling to a $G\beta\gamma_{i/o}$-PLCβ-IP_3-Ca^{2+}-calcineurin pathway (Hernandez-Lopez et al., 2000). The corresponding transduction cascades have not yet been defined in PD, but $D_{2\alpha Pan}$ can decrease cAMP concentration via $G\alpha_{i/o}$ and couple with PLCβ via $G\beta\gamma_{i/o}$ subunits in human embryonic kidney (HEK) cell lines (Clark and Baro, 2007).

DARs can also modulate ligand-gated ion channels. MSN D_2 receptors alter ionotropic excitatory glutamate receptors (GLURs) over multiple time scales (Kauer and Malenka, 2007; Kreitzer and Malenka, 2008; Shen et al., 2008). They acutely reduce the response to glutamate by promoting calcineurin-dependent AMPA receptor trafficking out of the synapse (Surmeier et al., 2007), and by inhibiting NMDA receptors through direct physical interactions (Liu et al., 2006). D_2 receptors also promote long-term depression (LTD) by activating endocannabinoid production in postsynaptic spines (Kauer and Malenka, 2007). In contrast, STG neurons possess ionotropic inhibitory GLURs (iGLURs), which are ligand-gated chloride channels (Cleland and Selverston, 1995, 1997, 1998). DA reduces glutamate-mediated currents in STG neurons, although it is not clear whether this is mediated by D_1 and/or D_2 receptors (Cleland and Selverston, 1997).

DARs may also continuously regulate the genetic program. Blocking striatal MSN D_2 receptors alters histone phosphorylation, and thereby chromatin structure (Stipanovich et al., 2008; Bertran-Gonzalez et al., 2009). Additionally, psychostimulant-induced prolonged elevations in DA generate long-term alterations in ion current density in striatal MSNs (Hu, 2007); however, this may be an indirect effect resulting from homeostatic adaptations to DA-induced changes in neuronal activity (Marder and Goaillard, 2006). In the STG, neuromodulators are known to regulate ion current densities continuously (Khorkova and Golowasch, 2007), but it is not clear whether this occurs at the transcriptional level, and the specific effects of DA are unknown.

D_2 receptor function in specific subcellular compartments of PD and striatal MSNs

Striatal MSNs and PD differ in a number of important respects, and yet, D_2 receptors modulate ion channels to decrease neuronal excitability acutely in both cell types. The data suggest that receptor locations may be reconfigured to accommodate significant differences in neuronal function and proteomes. For example, it appears that D_2 receptors reduce MSN and PD output either by inhibiting excitatory input or presynaptic release, respectively, and dendritic D_2 receptors may regulate spike timing-dependent (STD) plasticity in MSNs but not PD.

Whereas both cell types receive glutamatergic transmissions, postsynaptic GLURs are excitatory in MSNs and inhibitory in PD neurons. Thus, to reduce neuronal excitability, glutamatergic transmission should be inhibited in MSNs versus potentiated in PD. In fact, there are data showing that this occurs. MSN D_2 receptors are located on postsynaptic spines and function to reduce glutamatergic transmission, in part by reducing GLUR function, as previously described. On the other hand, it is not clear whether D_2 receptors are located on PD postsynaptic spines and/or whether they couple with iGLURs. However, it has been demonstrated that bath-applied DA increases the strength of the graded LP glutamatergic synapse onto the PD neuron, at least in part by increasing transmitter release through an unknown presynaptic mechanism, e.g.,

activate D_1 receptors on LP terminals (Johnson et al., 1995; Johnson and Harris-Warrick, 1997).

$D_{2\alpha Pan}$ receptors are located on PD presynaptic terminals, where they can reduce release by inhibiting I_{Ca} and increasing outward K^+ currents, as previously described. In contrast, D_2 receptors are not found on the axon terminals of MSNs projecting to the globus pallidus, which receives DA innervation (Yung et al., 1995). To our knowledge, there have been no reports examining DAR distribution on MSN axon collaterals that synapse locally (Taverna et al., 2008).

MSNs rely on spike-evoked transmission, whereas graded transmission predominates in the STG neuropil (Graubard et al., 1980, 1983). It has been suggested that one major function of DARs on MSN somata and dendritic shafts is to modulate I_A, which in turn regulates action potential back-propagation (Chen et al., 2006), and thereby STD plasticity (Luu and Malenka, 2008). In PD neurons, the channels mediating I_A are distributed throughout the somatodendritic compartment (Baro et al., 2000), but we did not observe surface $D_{2\alpha Pan}$ receptors on neurites or somata. It may be that our antibody could not detect these receptors. Alternatively, receptors in the terminals may generate global signals that regulate I_A throughout the somatodendritic compartment. It is also possible that whereas STD plasticity is found in inhibitory circuits (Caporale and Dan, 2008), it is less important in an inhibitory circuit in which graded transmission predominates.

CONCLUSIONS

In sum, D_2 receptors may have evolved to reduce neuronal output by decreasing excitability and/or synaptic release. Consistent with the fact that signaling proteins and ion channel targets are well conserved across species, D_2 receptor activation has similar effects on ion currents in mammals and arthropods. In both species, receptors appear to be concentrated at synapses and receive volume transmission. However, D_2 receptors may be differentially positioned at pre- versus postsynaptic processes in the two cell types to accommodate differences in cell function and proteomes. Further studies are required to determine the extent to which subcellular receptor distributions are altered to produce similar results in divergent cell types.

ACKNOWLEDGMENTS

We thank Hongmei Zhang and Tim Dever for technical assistance, and Brian Antonsen for advice on using the Neurolucida program. Figure 2A was illustrated by Sonia Hilliard, DVM (http://graphitegirl.shutterfly.com).

LITERATURE CITED

Agnati LF, Leo G, Zanardi A, Genedani S, Rivera A, Fuxe K, Guidolin D. 2006. Volume transmission and wiring transmission from cellular to molecular networks: history and perspectives. Acta Physiol (Oxf) 187:329–344.

Barker DL, Kushner PD, Hooper NK. 1979. Synthesis of dopamine and octopamine in the crustacean stomatogastric nervous system. Brain Res 161:99–113.

Baro DJ, Cole CL, Harris-Warrick RM. 1996. RT-PCR analysis of shaker, shab, shaw, and shal gene expression in single neurons and glial cells. Receptors Channels 4:149–159.

Baro DJ, Levini RM, Kim MT, Willms AR, Lanning CC, Rodriguez HE, Harris-Warrick RM. 1997. Quantitative single-cell-reverse transcription-PCR demonstrates that A-current magnitude varies as a linear function of shal gene expression in identified stomatogastric neurons. J Neurosci 17:6597–6610.

Baro DJ, Ayali A, French L, Scholz NL, Labenia J, Lanning CC, Graubard K, Harris-Warrick RM. 2000. Molecular underpinnings of motor pattern generation: differential targeting of shal and shaker in the pyloric motor system. J Neurosci 20: 6619-6630.

Beaulieu JM, Gainetdinov RR, Caron MG. 2009. Akt/GSK3 signaling in the action of psychotropic drugs. Annu Rev Pharmacol Toxicol 49:327–347.

Bertran-Gonzalez J, Hakansson K, Borgkvist A, Irinopoulou T, Brami-Cherrier K, Usiello A, Greengard P, Herve D, Girault JA, Valjent E, Fisone G. 2009. Histone H3 phosphorylation is under the opposite tonic control of dopamine D2 and adenosine A2A receptors in striatopallidal neurons. Neuropsychopharmacology 34:1710–1720.

Bockaert J, Fagni L, Dumuis A, Marin P. 2004. GPCR interacting proteins (GIP). Pharmacol Ther 103:203–221.

Bucher D, Thirumalai V, Marder E. 2003. Axonal dopamine receptors activate peripheral spike initiation in a stomatogastric motor neuron. J Neurosci 23:6866–6875.

Bucher D, Johnson CD, Marder E. 2007. Neuronal morphology and neuropil structure in the stomatogastric ganglion of the lobster, *Homarus americanus*. J Comp Neurol 501:185–205.

Cabello N, Gandia J, Bertarelli DC, Watanabe M, Lluis C, Franco R, Ferre S, Lujan R, Ciruela F. 2009. Metabotropic glutamate type 5, dopamine D(2) and adenosine a(2a) receptors form higher-order oligomers in living cells. J Neurochem 109: 1497–1507.

Caporale N, Dan Y. 2008. Spike timing-dependent plasticity: a Hebbian learning rule. Annu Rev Neurosci 31:25–46.

Cepeda C, Levine MS. 2006. Where do you think you are going? The NMDA-D1 receptor trap. Sci STKE 2006(333):pe20.

Chen X, Yuan LL, Zhao C, Birnbaum SG, Frick A, Jung WE, Schwarz TL, Sweatt JD, Johnston D. 2006. Deletion of Kv4.2 gene eliminates dendritic A-type K+ current and enhances induction of long-term potentiation in hippocampal CA1 pyramidal neurons. J Neurosci 26:12143–12151.

Clark M, Baro D. 2006. Cloning and characterization of crustacean type one dopamine receptors: D1aPan and D1bPan. Comp Biochem Physiol B Biochem Mol Biol 143:294–301.

Clark MC, Baro DJ. 2007. Arthropod D2 receptors positively couple with cAMP through the Gi/o protein family. Comp Biochem Physiol 146:9–19.

Clark MC, Dever TE, Dever JJ, Xu P, Rehder V, Sosa MA, Baro DJ. 2004. Arthropod 5-HT2 receptors: a neurohormonal receptor in decapod crustaceans that displays agonist independent activity resulting from an evolutionary alteration to the DRY motif. J Neurosci 24:3421–3435.

Clark MC, Khan R, Baro DJ. 2008. Crustacean dopamine receptors: localization and G protein coupling in the stomatogastric ganglion. J Neurochem 104:1006–1019.

Cleland TA, Selverston AI. 1995. Glutamate-gated inhibitory currents of central pattern generator neurons in the lobster stomatogastric ganglion. J Neurosci 15:6631–6639.

Cleland TA, Selverston AI. 1997. Dopaminergic modulation of inhibitory glutamate receptors in the lobster stomatogastric ganglion. J Neurophysiol 78:3450–3452.

Cleland TA, Selverston AI. 1998. Inhibitory glutamate receptor channels in cultured lobster stomatogastric neurons. J Neurophysiol 79:3189–3196.

Collins MO, Grant SG. 2007. Supramolecular signalling complexes in the nervous system. Subcell Biochem 43:185–207.

Cooper RL, Hampson DR, Atwood HL. 1995. Synaptotagmin-like expression in the motor nerve terminals of crayfish. Brain Res 703:214–216.

Cournil I, Helluy SM, Beltz BS. 1994. Dopamine in the lobster *Homarus gammarus*. I. Comparative analysis of dopamine and tyrosine hydroxylase immunoreactivities in the nervous system of the juvenile. J Comp Neurol 344:455–469.

Cournil I, Casasnovas B, Helluy SM, Beltz BS. 1995. Dopamine in the lobster *Homarus gammarus*: II. Dopamine-immunoreactive neurons and development of the nervous system. J Comp Neurol 362:1–16.

Flamm RE, Harris-Warrick RM. 1986a. Aminergic modulation in lobster stomatogastric ganglion. I. Effects on motor pattern and activity of neurons within the pyloric circuit. J Neurophysiol 55:847–865.

Flamm RE, Harris-Warrick RM. 1986b. Aminergic modulation in lobster stomatogastric ganglion. II. Target neurons of dopamine, octopamine, and serotonin within the pyloric circuit. J Neurophysiol 55:866–881.

Fonseca JM, Lambert NA. 2009. Instability of a class A GPCR oligomer interface. Mol Pharmacol 75:1296–1299.

Fort TJ, Brezina V, Miller MW. 2004. Modulation of an integrated central pattern generator-effector system: dopaminergic regulation of cardiac activity in the blue crab *Callinectes sapidus*. J Neurophysiol 92:3455–3470.

Goldstone MW, Cooke IM. 1971. Histochemical localization of monoamines in the crab central nervous system. Z Zellforsch Mikrosk Anat 116:7–19.

Goto Y, Grace AA. 2005. Dopaminergic modulation of limbic and cortical drive of nucleus accumbens in goal-directed behavior. Nat Neurosci 8:805–812.

Goto Y, Grace AA. 2008. Limbic and cortical information processing in the nucleus accumbens. Trends Neurosci 31:552–558.

Goto Y, Otani S, Grace AA. 2007. The Yin and Yang of dopamine release: a new perspective. Neuropharmacology 53:583–587.

Graubard K, Raper JA, Hartline DK. 1980. Graded synaptic transmission between spiking neurons. Proc Natl Acad Sci U S A 77:3733–3735.

Graubard K, Raper JA, Hartline DK. 1983. Graded synaptic transmission between identified spiking neurons. J Neurophysiol 50:508–521.

Guo X, Hartemink AJ. 2009. Domain-oriented edge-based alignment of protein interaction networks. Bioinformatics 25: i240–246.

Harris-Warrick RM, Johnson BR, Peck JH, Kloppenburg P, Ayali A, Skarbinski J. 1998. Distributed effects of dopamine modulation in the crustacean pyloric network. Ann N Y Acad Sci 860:155–167.

Hearn MG, Ren Y, McBride EW, Reveillaud I, Beinborn M, Kopin AS. 2002. A *Drosophila* dopamine 2-like receptor: molecular characterization and identification of multiple alternatively spliced variants. Proc Natl Acad Sci U S A 99:14554–14559.

Hernandez-Lopez S, Tkatch T, Perez-Garci E, Galarraga E, Bargas J, Hamm H, Surmeier DJ. 2000. D2 dopamine receptors in striatal medium spiny neurons reduce L-type Ca2+ currents and excitability via a novel PLCβ1-IP3-calcineurin-signaling cascade. J Neurosci 20:8987–8995.

Hersch SM, Ciliax BJ, Gutekunst CA, Rees HD, Heilman CJ, Yung KK, Bolam JP, Ince E, Yi H, Levey AI. 1995. Electron microscopic analysis of D1 and D2 dopamine receptor proteins in the dorsal striatum and their synaptic relationships with motor corticostriatal afferents. J Neurosci 15:5222–5237.

Hu XT. 2007. Cocaine withdrawal and neuro-adaptations in ion channel function. Mol Neurobiol 35:95–112.

Johnson BR, Harris-Warrick RM. 1990. Aminergic modulation of graded synaptic transmission in the lobster stomatogastric ganglion. J Neurosci 10:2066–2076.

Johnson BR, Harris-Warrick RM. 1997. Amine modulation of glutamate responses from pyloric motor neurons in lobster stomatogastric ganglion. J Neurophysiol 78:3210–3221.

Johnson BR, Peck JH, Harris-Warrick RM. 1993. Amine modulation of electrical coupling in the pyloric network of the lobster stomatogastric ganglion. J Comp Physiol [A] 172:715–732.

Johnson BR, Peck JH, Harris-Warrick RM. 1995. Distributed amine modulation of graded chemical transmission in the pyloric network of the lobster stomatogastric ganglion. J Neurophysiol 74:437–452.

Kabbani N, Levenson R. 2007. A proteomic approach to receptor signaling: molecular mechanisms and therapeutic implications derived from discovery of the dopamine D2 receptor signalplex. Eur J Pharmacol 572:83–93.

Kauer JA, Malenka RC. 2007. Synaptic plasticity and addiction. Nat Rev Neurosci 8:844–858.

Khorkova O, Golowasch J. 2007. Neuromodulators, not activity, control coordinated expression of ionic currents. J Neurosci 27:8709–8718.

Kilman VL, Marder E. 1996. Ultrastructure of the stomatogastric ganglion neuropil of the crab, *Cancer borealis*. J Comp Neurol 374:362–375.

King DG. 1976a. Organization of crustacean neuropil. I. Patterns of synaptic connections in lobster stomatogastric ganglion. J Neurocytol 5:207–237.

King DG. 1976b. Organization of crustacean neuropil. II. Distribution of synaptic contacts on identified motor neurons in lobster stomatogastric ganglion. J Neurocytol 5:239–266.

Klagges BR, Heimbeck G, Godenschwege TA, Hofbauer A, Pflugfelder GO, Reifegerste R, Reisch D, Schaupp M, Buchner S, Buchner E. 1996. Invertebrate synapsins: a single gene codes for several isoforms in *Drosophila*. J Neurosci 16:3154–3165.

Kloppenburg P, Levini RM, Harris-Warrick RM. 1999. Dopamine modulates two potassium currents and inhibits the intrinsic firing properties of an identified motor neuron in a central pattern generator network. J Neurophysiol 81:29–38.

Kloppenburg P, Zipfel WR, Webb WW, Harris-Warrick RM. 2000. Highly localized Ca(2+) accumulation revealed by multiphoton microscopy in an identified motoneuron and its modulation by dopamine. J Neurosci 20:2523–2533.

Kloppenburg P, Zipfel WR, Webb WW, Harris-Warrick RM. 2007. Heterogeneous effects of dopamine on highly localized, voltage-induced Ca2+ accumulation in identified motoneurons. J Neurophysiol 98:2910–2917.

Kreitzer AC, Malenka RC. 2008. Striatal plasticity and basal ganglia circuit function. Neuron 60:543–554.

Kushner PD, Barker DL. 1983. A neurochemical description of the dopaminergic innervation of the stomatogastric ganglion of the spiny lobster. J Neurobiol 14:17–28.

Liu XY, Chu XP, Mao LM, Wang M, Lan HX, Li MH, Zhang GC, Parelkar NK, Fibuch EE, Haines M, Neve KA, Liu F, Xiong ZG, Wang JQ. 2006. Modulation of D2R-NR2B interactions in response to cocaine. Neuron 52:897–909.

Luu P, Malenka RC. 2008. Spike timing-dependent long-term potentiation in ventral tegmental area dopamine cells requires PKC. J Neurophysiol 100:533–538.

Marder E, Bucher D. 2006. Understanding circuit dynamics using the stomatogastric nervous system of lobsters and crabs. Annu Rev Physiol 69:291–316.

Marder E, Goaillard JM. 2006. Variability, compensation and homeostasis in neuron and network function. Nature Rev 7:563–574.

Masri B, Salahpour A, Didriksen M, Ghisi V, Beaulieu JM, Gainetdinov RR, Caron MG. 2008. Antagonism of dopamine D2 receptor/beta-arrestin 2 interaction is a common property of clinically effective antipsychotics. Proc Natl Acad Sci U S A 105:13656–13661.

Mengual E, Pickel VM. 2004. Regional and subcellular compartmentation of the dopamine transporter and tyrosine hydroxylase in the rat ventral pallidum. J Comp Neurol 468:395–409.

Neve KA, Seamans JK, Trantham-Davidson H. 2004. Dopamine receptor signaling. J Recept Signal Transduct Res 24:165–205.

Nicola SM, Surmeier J, Malenka RC. 2000. Dopaminergic modulation of neuronal excitability in the striatum and nucleus accumbens. Annu Rev Neurosci 23:185–215.

Nikolaev VO, Bunemann M, Schmitteckert E, Lohse MJ, Engelhardt S. 2006. Cyclic AMP imaging in adult cardiac myocytes reveals far-reaching beta1-adrenergic but locally confined beta2-adrenergic receptor-mediated signaling. Circ Res 99:1084–1091.

Perez MF, White FJ, Hu XT. 2006. Dopamine D(2) receptor modulation of K(+) channel activity regulates excitability of nucleus accumbens neurons at different membrane potentials. J Neurophysiol 96:2217–2228.

Pulver SR, Marder E. 2002. Neuromodulatory complement of the pericardial organs in the embryonic lobster, *Homarus americanus*. J Comp Neurol 451:79–90.

Pulver SR, Thirumalai V, Richards KS, Marder E. 2003. Dopamine and histamine in the developing stomatogastric system of the lobster *Homarus americanus*. J Comp Neurol 462:400–414.

Schultz W. 2007. Multiple dopamine functions at different time courses. Annu Rev Neurosci 30:259–288.

Selverston AI, Russell DF, Miller JP. 1976. The stomatogastric nervous system: structure and function of a small neural network. Prog Neurobiol 7:215–290.

Shen W, Flajolet M, Greengard P, Surmeier DJ. 2008. Dichotomous dopaminergic control of striatal synaptic plasticity. Science 321:848–851.

Skiebe P, Ganeshina O. 2000. Synaptic neuropil in nerves of the crustacean stomatogastric nervous system: an immunocytochemical and electron microscopical study. J Comp Neurol 420:373–397.

Stipanovich A, Valjent E, Matamales M, Nishi A, Ahn JH, Maroteaux M, Bertran-Gonzalez J, Brami-Cherrier K, Enslen H, Corbille AG, Filhol O, Nairn AC, Greengard P, Herve D, Girault JA. 2008. A phosphatase cascade by which rewarding stimuli control nucleosomal response. Nature 453:879–884.

Strange PG. 2005. Oligomers of D2 dopamine receptors: evidence from ligand binding. J Mol Neurosci 26:155–160.

Sullivan JM, Benton JL, Sandeman DC, Beltz BS. 2007. Adult neurogenesis: a common strategy across diverse species. J Comp Neurol 500:574–584.

Sullivan RE, Friend BJ, Barker DL. 1977. Structure and function of spiny lobster ligamental nerve plexuses: evidence for synthesis, storage, and secretion of biogenic amines. J Neurobiol 8:581–605.

Sun ZY, Kauderer B, Schacher S. 1996. Differential distribution of functional receptors for neuromodulators evoking short-term heterosynaptic plasticity in *Aplysia* sensory neurons. J Neurosci 16:7540–7549.

Surmeier DJ, Ding J, Day M, Wang Z, Shen W. 2007. D1 and D2 dopamine-receptor modulation of striatal glutamatergic signaling in striatal medium spiny neurons. Trends Neurosci 30:228–235.

Taverna S, Ilijic E, Surmeier DJ. 2008. Recurrent collateral connections of striatal medium spiny neurons are disrupted in models of Parkinson's disease. J Neurosci 28:5504–5512.

Thuma JB, White WE, Hobbs KH, Hooper SL. 2009. Pyloric neuron morphology in the stomatogastric ganglion of the lobster, *Panulirus interruptus*. Brain Behav Evol 73:26–42.

Tierney AJ, Kim T, Abrams R. 2003. Dopamine in crayfish and other crustaceans: distribution in the central nervous system and physiological functions. Microsc Res Tech 60:325–335.

Tirotta E, Fontaine V, Picetti R, Lombardi M, Samad TA, Oulad-Abdelghani M, Edwards R, Borrelli E. 2008. Signaling by dopamine regulates D2 receptors trafficking at the membrane. Cell Cycle 7:2241–2248.

Ullah H, Scappini EL, Moon AF, Williams LV, Armstrong DL, Pedersen LC. 2008. Structure of a signal transduction regulator, RACK1, from *Arabidopsis thaliana*. Protein Sci 17:1771–1780.

Vomel M, Wegener C. 2008. Neuroarchitecture of aminergic systems in the larval ventral ganglion of *Drosophila melanogaster*. PLoS One 3:e1848.

Wilensky AE, Baldwin DH, Christie AE, Graubard K. 2003. Stereotyped neuropil branching of an identified stomatogastric motor neuron. J Comp Neurol 466:554–563.

Yao WD, Spealman RD, Zhang J. 2008. Dopaminergic signaling in dendritic spines. Biochem Pharmacol 75:2055–2069.

Yung KK, Bolam JP, Smith AD, Hersch SM, Ciliax BJ, Levey AI. 1995. Immunocytochemical localization of D1 and D2 dopamine receptors in the basal ganglia of the rat: light and electron microscopy. Neuroscience 65:709–730.

Zaccolo M, Pozzan T. 2002. Discrete microdomains with high concentration of cAMP in stimulated rat neonatal cardiac myocytes. Science (New York, NY) 295:1711–1715.

Zaslavskiy M, Bach F, Vert JP. 2009. Global alignment of protein-protein interaction networks by graph matching methods. Bioinformatics 25:i259–267.

Zoli M, Torri C, Ferrari R, Jansson A, Zini I, Fuxe K, Agnati LF. 1998. The emergence of the volume transmission concept. Brain Res Brain Res Rev 26:136–147.